support a quantitative prediction; but qualitatively, if the ice crystals show some degree of alinement, it should be possible to calculate their size and number by measuring their depolarizing effects at two frequencies using linear polarization. If ice-crystal orientation is random, their effects in circular polarization may be a good indication of their number and composition.

The high degree of stability of the background signal can be used to allow accurate studies of gaseous atmospheric constituents. The scintillations in the signal, if detectable, would provide a clue to the observation of atmospheric turbulence. Heavy precipitation should be detectable by this means if the signal is stable and well calibrated in amplitude. The total water content could be determined by observing and measuring signal absorption. It might be possible to measure the vertical distribution of a constituent by taking advantage of the pressure broadening of its absorption lines, using a forward-propagated signal at multiple wavelengths. One might even sweep the transmitted signal frequency across an absorption band to provide a complete frequency sample of the shape of the band of some particular molecule of interest. By choosing different absorption bands that are characteristic of different constituents, one could measure the specific atmospheric constituents individually.

PART B

ADDITIONAL APPLICATIONS AND RELATED TOPICS

THE MEASUREMENT OF SURFACE PRESSURE FROM A SATELLITE BY ACTIVE MICROWAVE TECHNIQUES

Although it is now possible to map the temperature structure of the atmosphere from satellites, pressure measurements are still limited by the coverage of ground-based instruments. More data are required from wider areas as an input to long-period numerical forecasts. Satellite methods for pressure measurement should be investigated. The following data requirements for a set of global meteorological measurements sufficiently accurate to provide initial conditions for a numerical forecast up to 2 or 3 weeks ahead have been specified by GARP (ref. 4–62):

1. Wind components: ± 3 m/sec
2. Temperature: ± 1 K
3. Pressure of reference level: ± 0.3 percent
4. Water vapor pressure: ± 100 N/m^2
5. Time average interval: 2 hr
6. Horizontal space average: 100 km
7. Vertical space average: eight levels at 100 000, 90 000, 70 000, 50 000, 20 000, 10 000, 5000, and 1000 N/m^2, respectively.

Such a vast amount of data can possibly be collected in the necessary time and at a reasonable cost only by the use of remote-sounding instruments on satellites. Although a geostationary satellite provides the most convenient platform for such closely spaced observations, it has the disadvantage of being at a very large distance (36 000 km), so that the antenna size required to achieve an acceptable ground resolution or to intercept sufficient energy of a return echo may be prohibitive. Therefore, for the purpose of this discussion, it is assumed that the instrument is mounted on a satellite orbiting at approximately 1000 km.

An accuracy of ± 0.3 percent in a pressure measurement corresponds to a height change of only 20 m, so that the height at which the pressure is measured must be known to within this value. This requirement renders the measurement of the three-dimensional pressure field very difficult. In principle, the desired accuracy might be achieved by a radar or lidar technique, but any pressure-

dependent contributions to atmospheric backscatter are so weak that measurement is impossible with reasonable source powers and receiver apertures. This leaves only methods that measure surface pressure. Of course, the hydrostatic approximation, in conjunction with the measured temperature field, will allow reconstruction of the entire pressure field from the surface pressure, so that the restriction is not serious.

It has been proposed that atmospheric pressure could be deduced from measurements of the optical length of a path through the atmosphere. In practice, the dispersion between two different wavelengths must be measured. Unfortunately, this effect is very small. In the visible spectrum, dispersion can give a time difference of approximately 5×10^{-10} sec, and calculations by Liebe (ref. 4–63) give rather smaller times in the 5-mm O_2 band. To measure pressure to 0.3 percent, the time resolution must be approximately 1.5×10^{-12} sec. This is many orders of magnitude less than the equivalent length of a pulse reflected from the ocean surface (waves of 5 m in depth are equivalent to a time difference of approximately 3×10^{-8} sec). The only practical method for achieving such resolutions is to have separate transmitting and receiving stations on satellites, so spaced that the path between them includes some of the atmosphere. One would probably measure the phase of a continuous signal rather than timing the arrival of a pulse. Such a technique is not possible for reflection from the ocean surface, because the roughness of the surface renders the echo incoherent.

The most promising methods for surface-pressure measurement depend on measuring the intensity of energy reflected from the surface both in an atmospheric absorption band and at a nearby wavelength. The attenuation of the light in the atmosphere by Rayleigh scattering in clouds and the surface reflectivity are slowly varying functions of wavelength. Therefore, the ratio of the intensities at the two wavelengths is a measure of the atmospheric absorption due to the absorption band, from which the total amount of gas in the atmosphere and, hence, the surface pressure can be deduced.

The chosen absorption band must be due to a major constituent (e.g., O_2). Absorption bands of variable minor constituents such as water vapor or ozone must be avoided. Even CO_2 is probably not sufficiently evenly mixed for this purpose. Possible microwave O_2 bands occur at 0.76 μm and 5 mm.

Under favorable conditions, the absorption will need to be measured to 1 part in 80 to achieve the required accuracy of 300 N/m^2 in the surface pressure. (See the section entitled "Water Vapor.")

The Sun does not provide a suitable source at either wavelength. At 0.76 μm, under broken-cloud conditions, a substantial amount of sunlight is reflected back from the cloud top and does not traverse the entire atmosphere. (This fact has been used to determine cloud-top altitude.) An active, pulsed source allows discrimination against such cloud reflections. At 5 mm, the cloud reflectivity is negligible; but the Sun reflected in the rough ocean surface provides a signal weaker than thermal emission from the ocean and atmosphere, from which it cannot be distinguished. An active manmade source is then required. For the purpose of numerical estimates of minimum-required transmitter power, reflection at normal incidence from the ocean surface is considered. Rather higher powers would be required for operation over a land surface or over the oceans at nonnormal incidence.

At 0.76 μm, the most practical source is probably a dye laser pumped by either a flash lamp or a ruby laser. If a 1-J pulse (4×10^{18} photons) is assumed, the number of photons returned into an entrance aperture of 30 cm at a satellite height of 1000 km can be deduced from the ocean-surface reflectivity calculated by Krishen (ref. 4–64). The fraction returned is approximately 1.5×10^{-13} or 6×10^{5} photons. If the atmospheric transmission is 0.37 and if a photomultiplier with a quantum efficiency of 0.1 is used, the number of photoelectrons will be 2×10^{4} and the accuracy of intensity measurement will be $1/(2\times10^{4})^{1/2}$

$=1/140$. This assumes (1) that reflected sunlight can be reduced to a negligible amount by filtering and using a narrow field of view, and (2) that dark current in the photomultiplier is eliminated by cooling the tube, if necessary.

The overall efficiency of the laser system is unlikely to exceed 0.05 percent, so that 2000 J of electrical energy would have to be stored (400 μF at 3300 V). If a measurement is required every 10 sec, the power consumption would be 200 W. In addition to this high power consumption, the lifetime of the flash tube (approximately 10^5 flashes) may present a problem. However, the method seems feasible in principle, but it compares poorly with other methods discussed in this report.

This method has been previously investigated by Singer (ref. 4–65). Singer concludes that rather high power would be needed, but his calculations are based on a "gray" surface with albedo 0.1, which gives a value of 3×10^{-15} for the fraction of power returned compared with 1.5×10^{-13} from Krishen's calculation (ref. 4–64) for an ocean reflectivity.

At a frequency of 50 GHz, solid-state sources can provide powers approaching 1-W continuous wave (ref. 4–66), whereas vacuum devices can provide more if necessary.

The return signal from a 1-W transmitter is calculated to be approximately 5×10^{-3} W into a receiver aperture of 30-cm diameter. (The reflectivity is higher in the microwave region than in the visible region because of the larger dielectric constant of water.) If the receiver and blackbody source are at temperature T, if the intermediate-frequency bandwidth is Δf, and if the time constant after rectification is t, then noise-equivalent power is $4kT(\Delta f/t)^{1/2}F$, where k is the Boltzmann constant and F is the noise factor of the receiver (approximately 10 in practice). (The Rayleigh-Jeans' approximation for the blackbody radiation function is applicable to the microwave part of the spectrum.) Assuming an intermediate-frequency bandwidth of 30 MHz and assuming an integrating time constant of 1 sec, the SNR is 500:1, which should be adequate for the present purpose.

The O_2 5-mm band is the most promising for the proposed measurements; and, in the next section, atmospheric transmission in this region of the spectrum is considered in detail.

Atmospheric Transmission and Ocean Reflectivity in the Neighborhood of the 5-mm Oxygen Band

This section considers several factors that will affect the received signal strength. At normal incidence, the ocean reflection is predominantly specular if the surface structure is large compared with the radiation wavelength (ref. 4–64). Waves on the ocean surface cause an angular spread in the reflected radiation so that the proportion of the reflected energy intercepted by the receiver entrance aperture decreases as the wave amplitude increases. From Krishen's results (ref. 4–64), values for the radar-scattering coefficient σ° of 18 to 8 dB are obtained corresponding to sea states induced by wind of 5 to 25 m/sec. The fraction of incident power reflected into the receiver P_r is approximately related to σ° by

$$P_r \approx 0.28\left(\frac{d}{R}\right)\sigma^\circ \qquad (4\text{–}55)$$

where d is the aperture diameter and R is the radar range. The values quoted in the introduction of the section entitled "The Measurement of Surface Pressure From a Satellite by Active Microwave Techniques" correspond to an intermediate value for windspeeds of approximately 10 m/sec.

At normal incidence, there is only a slight variation in backscattering cross section with frequency due to dispersion in the dielectric constant. Away from normal incidence, the reflected power drops rapidly and varies with the roughness of the surface on a scale comparable with the wavelength, so that rather different behavior is expected. It is assumed that measurements are to be made at or near normal incidence.

There will be some fluctuation of the inten-

sity of the reflected power with time. To reduce the effects of those fluctuations, it is necessary to average a number of independent measurements at each frequency and to insure that the different frequencies are measured close together in time.

Although the 5-mm O_2 band has a complicated structure caused by rotational transitions between magnetic-line structure levels, in the wings of the band the absorption can be represented by a single Lorentz line. To obtain the most sensitive measure of surface pressure, it will be shown that the transmission on a double pass through the atmosphere should be e^{-1}. This occurs at a frequency of about 50 GHz (the band center is at 60 GHz), where the single-line approximation should apply. The pressure and temperature dependence are given in equation (4–56), where the exponents have been chosen to match Liebe's (ref. 4–63) results obtained by detailed, line-by-line calculations:

$$k=\frac{C\left(\frac{p}{p_0}\right)^{x(\nu)}\left(\frac{T}{T_0}\right)^{y(\nu)}}{1+\left(\frac{\nu_c-\nu}{\gamma_c}\right)^2} \qquad (4\text{–}56)$$

Here, k is the atmospheric absorption coefficient, C is a constant, p is the pressure, T is the temperature, ν is the frequency, ν_c is the band center frequency, γ_c is the width of the Lorentz line, and p_0 and T_0 are standard pressure and temperature.

The transmission for a double pass through the atmosphere is $\tau=\exp(-A)$, where the zenith absorption $A=2\int_0^\infty k\,dz$ and z is the vertical coordinate.

The atmosphere is quite accurately in hydrostatic equilibrium so that

$$p_a g\ d_z=-dp \qquad (4\text{–}57)$$

where p_a is the density and g is the acceleration of gravity. This may be written

$$\frac{dz}{z_0}=-\frac{T}{T_0}\frac{dp}{p} \qquad (4\text{–}58)$$

where $z_0=(RT_0)/(M_m g)$ (for the scale height at temperature T_0, and where R is the gas constant and M_m is the mean molecular weight for the atmosphere). Hence

$$A=2z_0\int_0^{p_G} k\,\frac{T}{T_0}\frac{dp}{p} \qquad (4\text{–}59)$$

where p_G is the ground pressure and k is the atmospheric attenuation coefficient.

Most of the absorption will occur in the lower part of the atmosphere where the temperature falls approximately linearly with height. The dry adiabatic lapse rate is obtained by considering the temperature T that would be attained by a block of air if expanded adiabatically from the ground pressure p_G and ground temperature T_G to the pressure p at a particular height.

$$T=T_G\left(\frac{p}{p_G}\right)^q \qquad (4\text{–}60)$$

where $q=(\gamma_r-1)/\gamma_r\approx 0.3$ and $\gamma_r=C_p/C_v$ is the ratio of specific heats for air.

If $p/p_G\approx e^{-z/z_0}$ is substituted into equation (4–60) and the exponent is expanded, then

$$T\approx T_G\left(1-\frac{qz}{z_0}\right) \qquad (4\text{–}61)$$

Lapse rates other than dry adiabatic may be described by changing the value of q. Equation (4–59) may be evaluated by making use of equations (4–56) and (4–60) for T, such that

$$A=\frac{\frac{2az_0}{x+q(y+1)}\left(\frac{p_G}{p_0}\right)\left(\frac{T_G}{T_0}\right)^{y+1}}{1+\frac{\nu_c-\nu^2}{\gamma_c}} \qquad (4\text{–}62)$$

If detector noise is the limiting factor, the frequency of operation should be chosen to give maximum transmission variation with changes in ground pressure. This maximum occurs when $A=1$ at a frequency of 51 GHz, where $x=2$ and $y=-2.6$ (figs. 4–23 and 4–24). If the received signal is s, the sensitivity to variations in p_G, T_G, and q is given by

$$\frac{\Delta s}{s}=-2\left(\frac{\Delta p_G}{p_0}\right)+1.6\left(\frac{\Delta T_G}{T_0}\right)-\frac{0.8\Delta q}{1-0.8\Delta q} \qquad (4\text{–}63)$$

If the surface pressure is required to an accuracy of 300 N/m^2, $(\Delta s)/s$ is equal to ± 0.6

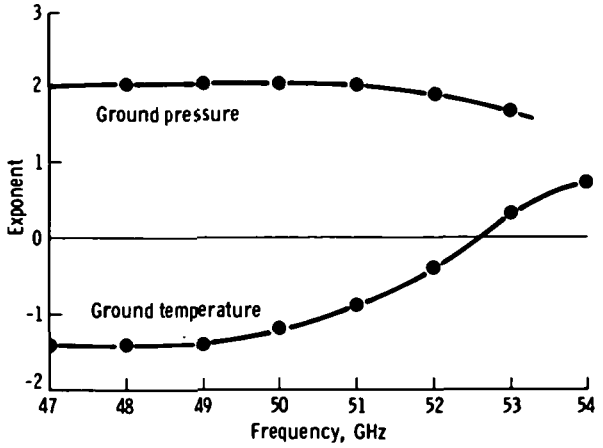

FIGURE 4–23.—Dependence of absorption coefficient on ground pressure and temperature.

percent and T_G must be known to ± 0.4 percent or 1 K and q to ± 0.006 (lapse rate of ± 0.25 deg/km).

This simple model is intended only to give an appreciation of the way the atmospheric transmission depends on ground pressure and atmospheric temperatures. In practice, corrections for possible temperature variations would have to be applied through a more precise model and through the pressure calibration obtained from passes over ground stations where surface pressure is accurately known.

It has been shown that in the wings of the 5-mm O_2 band, the absorption coefficient for the two-way pass through the atmosphere should vary as $p_G^2 T_G^{-1.6}$, so that quite accurate values for surface temperature are needed if surface pressure is to be deduced. The exponents of pressure and temperature as functions of frequency are plotted in figure 4–23. These detailed, line-by-line calculations were based on a standard atmosphere with a constant lapse rate, maintained in hydrostatic equilibrium as ground temperature is changed (fig. 4–25). Notice that at a frequency of 52.5 GHz, the atmospheric transmission becomes largely independent of temperature. This is further emphasized in figure 4–26, which shows the variations in ground temperature and in lapse rate that produce a change in atmospheric transmission equivalent to a 300-N/m² change in surface pressure. The transmission of the two-way pass through the atmosphere at 52.5 GHz is approximately 0.12; therefore, it is still quite feasible to operate an instrument

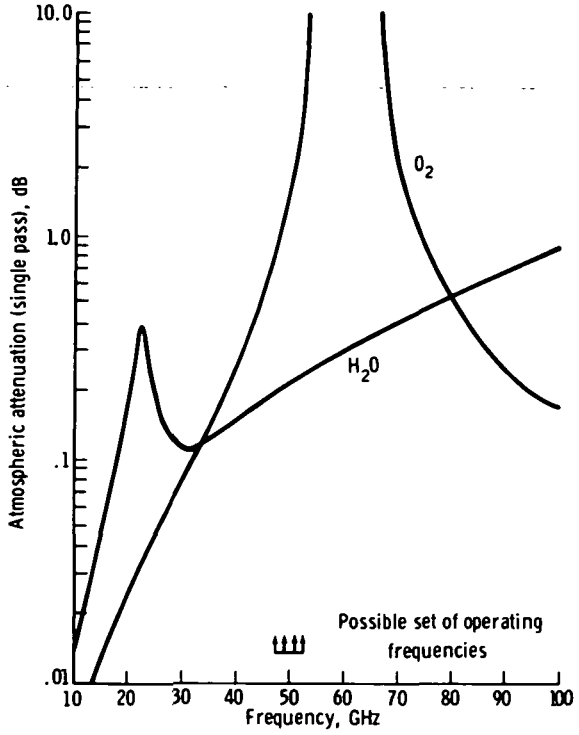

FIGURE 4–24.—Atmospheric O_2 and water vapor absorption.

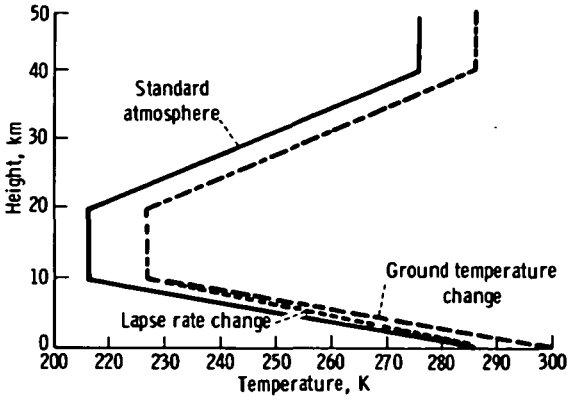

FIGURE 4–25.—Standard atmosphere and variation in T_G and lapse rate used in figure 4–23. (Variation exaggerated by a factor of 10.)

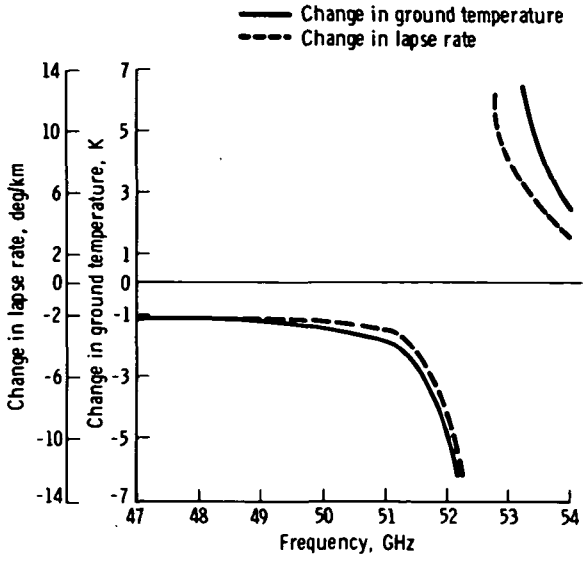

FIGURE 4–26.—Change in ground temperature and lapse rate to give atmospheric transmission change equal to 300-N/m² change in ground pressure.

at this frequency, even though this transmission is less than the optimum transmission for maximum sensitivity to surface pressure.

In fact, there are some advantages in moving farther into the absorption band. Although the absolute change in signal for a given pressure change is greater at an atmospheric transmission of e^{-1}, the fractional change increases with the absorption. At an overall transmission of 0.12, the signal needs only to be measured to a precision of 1 part in 80 for a 0.3-percent accuracy in pressure, compared with 1 part in 150 at transmission e^{-1}. The corrections for water-vapor absorption, cloud transmission, etc., then need be less accurate.

In table 4–VII, s is the received signal, s_0 is the signal that would be received in the absence of atmospheric absorption, and Δs is the change in s for a change Δp_G in surface pressure p_G.

Water-vapor absorption must be considered for the following reasons:

1. Water-vapor partial pressure makes a significant contribution to surface pressure (up to 500 to 800 N/m²).

2. Water-vapor absorption occurs at 50 GHz and must be allowed for, even if the interest is only evaluation of the O_2 absorption. Also, the presence of water vapor affects the middle of the O_2 lines and hence the O_2 absorption coefficient itself.

The first effect is quite small because of the total required accuracy of 300 N/m², and the water-vapor content could probably be estimated accurately enough without measurement.

The absorption caused by water vapor around 50 GHz is a slowly varying function of the absorption coefficient, being proportional to y^2, and could be included in the interpretation of cloud transmissivity and ocean reflectivity so that the amount of water vapor need not be known. The effect of changes in the width of the O_2 line caused by the presence of water vapor is small, but further calculations are necessary to determine whether a measurement of the water-vapor content would be required.

If such a measurement proved necessary, an instrument similar to the surface-pressure sounder could be built, operating over the 22-GHz water-vapor absorption band for example. Much lower precision would be needed for this measurement of the total water vapor.

Benoit (ref. 4–67) gives the following expression for the absorption coefficient of clouds in this region of the spectrum:

TABLE 4–VII.—*Attenuation at 2 Frequencies for a Double-Pass Atmospheric Transmission*

Frequency, GHz	Atmospheric transmission (double-pass)	Relative signal change $(\Delta s)/s$	Absolute signal change Δs
51.0.....	e^{-1}	$-2(\Delta p_G)/p_G$	$-0.74 s_0(\Delta p_G)/p_G$
52.5.....	0.12	$-3.7(\Delta p_G)/p_G$	$-.45 s_0(\Delta p_G)/p_G$

$$\alpha = \rho_c \nu^b e^a \qquad (4\text{–}64)$$

where ρ_c is the density of water in cloud in g/m^3, ν is the frequency, b is equal to 1.95 for a water cloud and 1.006 for ice, and the constant a depends on temperature. For water, $a = 6.866\ (1 + 0.6045T)$; for ice, $a = -8.261\ [1 - (1.767 \times 10^{-2}\ T) - (4.374 \times 10^{-4}\ T^2)]$, where T is in degrees Celsius. For the present purpose, it is sufficient to note that to remove the effects of cloud from the measurements, it will be necessary to allow for an absorption with components varying approximately as ν and as ν^2, in addition to the clear atmospheric absorption.

Although no detailed study has been made of attenuation caused by rain, it will be a smooth function of frequency, which can be allowed for by a polynomial similar to the cloud case over the range of frequencies of interest.

Proposed Instrument Concepts

The measurement of atmospheric transmission cannot be made absolutely, because the ocean-surface reflectivity and land transmissivity are unknown. In addition, such absolute measurements are technically extremely difficult because of variation in transmitter power and receiver sensitivity. The basic measurement will be the ratio of signal strengths at one or more pairs of frequencies sufficiently well separated so that the O_2 absorption differs substantially (i.e., the frequency separation must be approximately the width of the band, which is about 4.5 GHz). One pair of frequencies would suffice if cloud transmission and ocean-surface reflectivity were independent of frequency. Two pairs would be needed to allow a linear variation in these quantities with frequency.

The main difficulty in the design of the hardware is to devise a system architecture that provides equal transmitter power and receiver gain at both frequencies, because calibration to the required accuracy is probably beyond the state of the art. A possible approach is shown in figure 4–27. The transmitter chain consists of the output of an oscillator tuned at the mean frequency f_0 mixed with the output of a CW oscillator at half the difference frequency f_1, followed by a power amplifier. The sum and difference frequency outputs from the mixer are equal in amplitude, and the amplifier-antenna chain should have equal gain at the two frequencies. The receiver consists of a local oscillator at frequency $f_0 + \Delta f$, slightly offset from the mean frequency so that, at the output of the first mixer, the two frequencies $f_0 + f_1$ and $f_0 - f_1$ give rise to closely spaced components $f_1 \pm \Delta f$. These are reduced in frequency by a second mixer and passed through a common intermediate-frequency amplifier before being separated by filters, detected, and compared. Because the intermediate-frequency amplifier is common to both frequencies, gain drifts do not affect the final ratio.

Although the prime measurement will be relatively independent of temperature, it will be necessary to make some temperature corrections. The necessary temperature accuracy will be obtained as a result of more detailed calculations, but temperature will certainly not be required to an accuracy smaller than ± 1 K; probably much less accurate values will suffice. (See the section entitled "Atmospheric Transmission and Ocean Reflectivity in the Neighborhood of the 5-mm Oxygen Band.") Probably the most convenient source of such information would be a passive temperature sounder mounted on the same satellite. If such an instrument were available, it would be worth considering in some detail how the information from active and passive measurements might be combined to the benefit of both.

So far, the system has been described as a CW system making an overall transmission measurement. Some modulation will be necessary to distinguish the signal from thermal emission and to insure that the transmitter does not operate during reception of the echo. This transmission measurement could be affected by backscatter in the atmosphere from clouds and rain. Although the backscatter from clouds is probably negligible, backscatter from rain is possibly a significant factor.

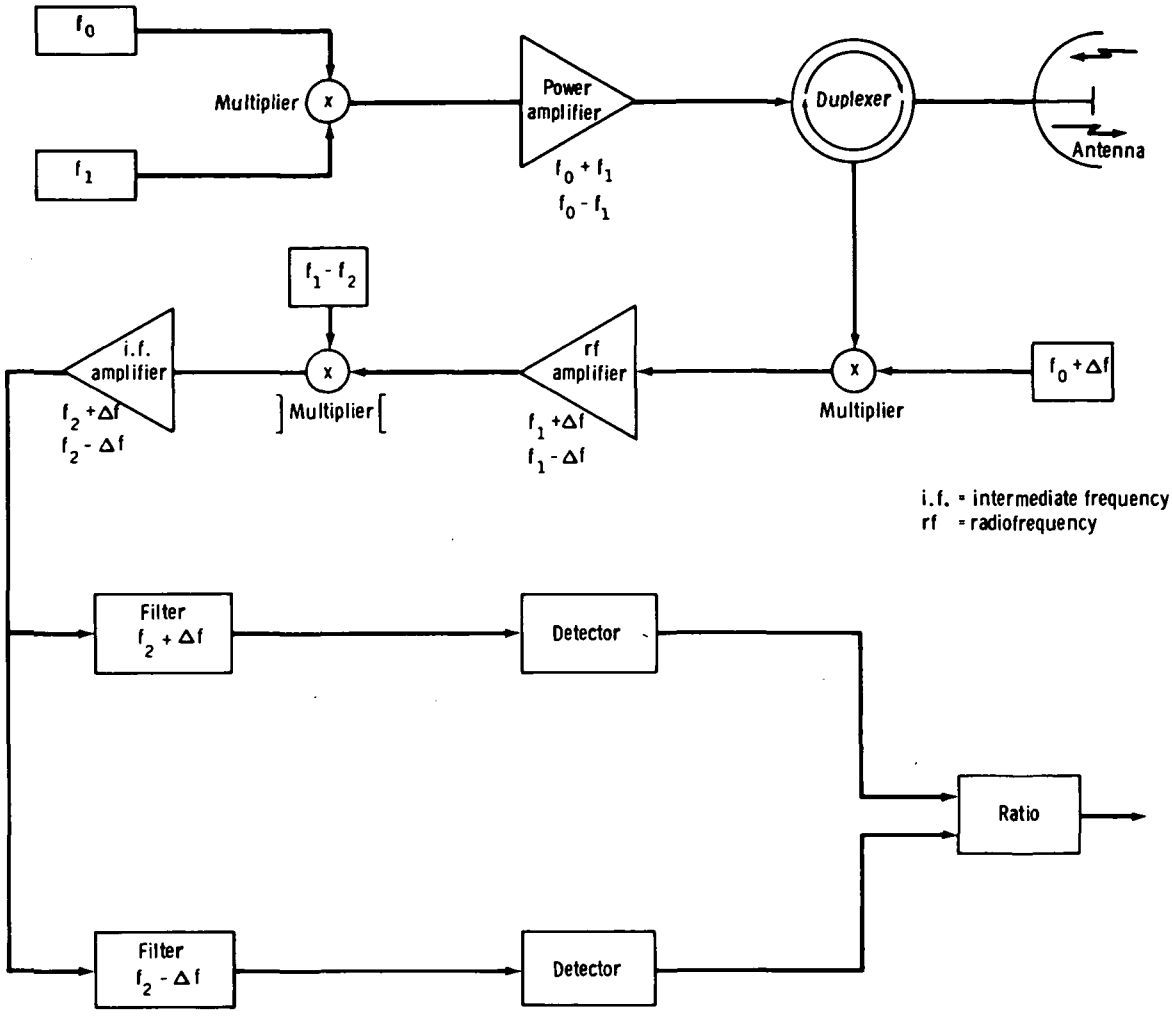

FIGURE 4–27.—Block diagram of possible transmitter and receiver configuration to obtain an accurate ratio of intensities at two frequencies.

Backscatter could be allowed for either source by estimating a correction or, instrumentally, by using a pulsed or coded source so that the surface echo may be distinguished by its time of travel.

Because the ocean reflectivity changes so rapidly as one scans away from normal incidence, unless a large increase in transmitter power or antenna size can be tolerated, the instrument will have to look vertically downward. This imposes a restriction on the ground coverage that can be achieved with a single satellite. A small scan of a few degrees might be accommodated; it would allow the pressure gradient and hence the geostrophic wind to be deduced. Larger transmitter powers and/or antenna sizes would also allow operation over land.

Summary

An active microwave sounder operating in the 5-mm O_2 absorption band and mounted on an Earth-orbiting satellite has been proposed as a means for the remote measurement of atmospheric surface pressure. At 52.5 GHz, the O_2 absorption has been shown to be largely independent of the temperature structure of the atmosphere, but depends strongly

on the surface pressure. A measure of the absolute transmissivity of the atmosphere at this frequency allows surface pressure to be deduced. Such a measurement can be made by reflecting a signal from a satellite transmitter off the ocean surface. Measurements at nearby frequencies allow the effects of varying ocean-surface reflectivity, clouds, and water vapor to be included.

The total water-vapor content of the atmosphere may also be measured by a similar instrument operating near the 22-GHz water-vapor absorption line.

METEOROLOGICAL APPLICATION OF SURFACE WINDS OVER OCEANS

The atmosphere panel noted with great interest the proposals for remote sensing of sea state with active microwave systems, especially the suggestions that wind direction, as well as windspeed at the surface, can be inferred. Surface wind information, if used in conjunction with a variational analysis scheme (such as that proposed by Y. Sasaki (ref. 4–68)), can greatly improve the initial analysis on which operational weather forecasts are based. Other applications include improved prediction of hurricanes and storm surges, and improved understanding of atmospheric processes.

This section is a review of (1) the capabilities that have already been demonstrated for inferring the surface wind from sea-state backscatter, (2) the unique advantages of determining surface winds in this way, and (3) the several NASA meteorological program objectives into which such wind determinations will fit. Finally, an estimate will be made of the meteorological benefits that would accrue from implementing a program to infer sea-surface winds from satellites.

Inference of Surface Wind From Backscatter

Earlier chapters of this report include reviews of previous experimental work relating radar backscatter to the windspeed and directions over the ocean. These are discussed specifically in chapter 3 in the section entitled "Large-Scale Phenomena." In summary, an empirical functional relationship between windspeed and radar cross section has been found. A smaller but significant dependence was also found between scattering cross section and the orientation of the wind. The results suggest that a four-beam array similar to an aircraft Doppler navigation system (but measuring backscattered power instead of Doppler shifts) could provide sufficient information to determine both windspeed and wind direction at the ocean surface. The signal disappears when the winds are nearly calm because of a lack of short-wavelength ocean waves. However, the absence of signal is a definite indication of light or calm winds. In very light winds, there is minimal interest in wind direction.

Meteorological Program Requirements for Winds Over Oceans From Satellite Microwave Systems

Over the oceans, surface windspeed alone can be inferred radiometrically, but determination of wind direction requires an active system. The determination of wind vector by Doppler techniques using the signal returned from precipitation particles (see the section entitled "Satellite-Borne Radar With Doppler Capability") is another possible means of determining winds with microwave systems. However, sufficiently large precipitation particles occupy only a small fraction of the atmosphere at any one time. Determining winds from sea-state condition is the only possible method, other than cloud motion, to obtain wind information from the nonprecipitating regions of the atmosphere.

Wind-velocity vectors inferred from the radar sea cross section can be considered as surface wind without ambiguity. In contrast, there can be considerable height uncertainty when winds are derived from cloud motions. For example, cloud elements are not truly conservative; and, therefore, pattern recognition schemes for tracking clouds are somewhat indefinite. Furthermore, it is not possible to be very accurate concerning the

infrared radiating temperature of cloud tops unless the cloud layer is a thick overcast. If tall cumulus towers are tracked, there is no unique way of knowing at what level the winds match the cloud motion.

There is a unique complementarity between winds determined from Doppler measurement of precipitation particles and winds inferred from sea state. This complementarity occurs because the same clutter that is essential for the operation of the Doppler technique would distort the backscatter signature from the sea surface. Thus, each technique works best when the other works least.

Three of the NASA meteorology program objectives would be served by having surface winds over ocean areas derived from wave backscatter. The first of these is weather prediction. A continuing objective in support of weather prediction is to develop the technology for determining the vertical structure of the atmosphere as an input into numerical prediction models. It has been shown recently (ref. 4–69) that knowing the vertical structure of the state variables (pressure, temperature, and composition) and the approximate time and space derivatives of these variables does not constitute sufficient information to update a numerical prediction model of the type used by most of the major weather centers. The measurement of the wind at one level within the atmosphere is also required. The determination of near-surface winds meets this requirement. Thus, a satellite with a payload similar to that planned for SEASAT–A could continuously provide the data set required to update numerical prediction models.

An additional application in support of numerical weather predictions would be an approximate extension to better coverage of the pressure-measuring scheme proposed in the section of this chapter entitled "The Measurement of Surface Pressure From a Satellite by Active Microwave Techniques." However, this measurement scheme would be considerably less sensitive at angles differing much from vertical incidence. Using the derived surface winds together with the geostrophic relationship would allow approximate reconstruction of the pressure gradient and thus the complete surface-pressure field. The application would require the observation of sea backscatter at several angles of incidence to obtain the wind measurement in the vicinity of the subpoint where the pressure measurements are made.

Operational numerical prediction models of the mid-1970's do not attempt to use wind data for the initial analysis. Instead, only pressures (or the height of constant pressure surfaces) are used to generate the assumed initial condition windspeeds. However, it is likely that, by the time an active microwave surface wind system is flown, the numerical prediction models may derive the initial condition windspeeds through a procedure such as Sasaki's (ref. 4–68) variational analysis scheme, which can use wind information as well as pressure information. A significant portion of the present error in weather predictions for more than 24 hr ahead can be attributed to an imperfect initial state of the numerical models. Any improvement of the fidelity of the initial conditions will certainly increase the accuracy of synoptic-scale weather forecasts in the realm of 2 to 6 days.

The second meteorology program objective served by the measurement of winds over the oceans is weather danger and disaster warning. Specifically, the winds surrounding hurricanes or typhoons can be measured. Empirical techniques are available for estimating maximum winds near the storm center from the character and diameter of the central, dense, cirrus overcast as viewed in visual wavelengths by satellite sensors. However, the primary consideration for public warning would be the distance that gale- or hurricane-force winds extend outward from the center; this distance is not uniquely determined by the maximum wind. The microwave system flown on Skylab 1 (experiment S193) successfully mapped a major section of the surface windfield of Hurricane Ava on June 5, 1973, in the eastern Pacific. Even if the windfield were measured only every 12 hr, such a measurement would supply a major

piece of warning information that is now missing (unless ships or aircraft are in the vicinity of the storm). In a prediction context, low-level wind data are most vital. For instance, measurement of winds in the lowest levels of a hurricane have had more value in modeling hurricane strength than winds measured higher in the storm (ref. 4–32).

Finally, the measurement of surface winds over the tropical oceans is necessary for a better understanding of tropical dynamic processes on scales between the single cumulus scale and the planetary scale. It is believed that a major factor in the development of cumulus clusters is the presence of large-scale divergence in the upper troposphere. It is normally assumed that there must be compensating convergence near the surface, but the low-level convergence has not been directly observed (because of a lack of suitably spaced wind measurements). The use of satellite-derived winds from wave backscatter offers the first opportunity to directly measure the low-level convergence.

Anticipated Results

Predicting the weather itself is more accurate than predicting improvements in forecasting models. However, a modest statement of anticipated results can be offered. Assuming the existence of an operational satellite family based on SEASAT–A technology, one could expect, by the early 1980's, to see an improvement resulting from the greater density of data over ocean areas. The improvement in forecasting will be most notable in the range of 3 to 6 days. It may then be possible to predict the general nature of the weather 4 or 5 days ahead with the same skill that meteorologists now have in forecasting 2 days ahead. A definite improvement in 1- to 2-day forecasts on the west coast should also be expected.

In the area of hurricane warning, it should be possible, a few years after SEASAT, to see definite improvements in the prediction of storm surges and the location of destructive winds once the storm is close enough for hurricane warnings. It is not possible to know at this time how much improvement might be expected in the form of reduced "watch" areas by better long-term prediction of a hurricane's path.

One can look forward to a considerably improved understanding of dynamic-scale interaction in the Tropics. This understanding (leading to better parametrization of the role of cumulus-scale clouds in the Tropics), when combined with the global capability to update numerical prediction models, will also lead to improved weather forecasts, especially in the range of 3 to 6 days ahead.

METEOROLOGICAL APPLICATIONS FOR SEA-ICE MAPPING IN POLAR REGIONS

The Earth-atmosphere system constitutes a large (and inefficient) heat engine. The Tropics can be considered the "fire box" of the engine, absorbing an excess of incident solar radiation compared to the long-wave radiation lost to space. The polar regions, however, lose more radiation to space than they receive from the Sun. The resultant meridional gradient of net (absorbed solar minus emitted long-wave) radiation ultimately results in the energy that drives the atmospheric and oceanic circulations.

Important factors governing the radiation lost to space in the polar regions (and, hence, the meridional gradient of the net radiation, which affects the energetics of the atmospheric circulation, in turn affecting weather and climate) are the interactions among air, ice, and water in the polar regions. For example, the flux of heat from the polar sea surface to the atmosphere can be as much as three orders of magnitude greater from open water than from ice cover.

The ESMR flown on Nimbus 5 in December 1972 has already provided much new knowledge concerning the gross characteristics of sea-ice morphology and dynamics. This instrument operates at a frequency of 19.35 GHz ($\lambda = 1.55$ cm) and has a spatial resolution of approximately 30 km. A similar instrument is scheduled to fly on Nimbus-F late in 1975.

Chapter 3 of this report discusses the additional requirement for high-resolution sequential imagery of selected areas to test existing and developing models for sea-ice dynamics and the energy exchange in the ice-water-atmosphere system. The type of instrument suggested by the ocean panel as being most suitable for these investigations is an SAR. The atmosphere panel endorses this recommendation by the ocean panel as one of interdisciplinary interest between the oceanic and atmospheric scientists.

MOLECULAR TRANSFER CHARACTERISTICS OF AIR BETWEEN 10 AND 150 GHz

Applications are dependent upon the ability to describe the somewhat complicated interaction between microwave energy and the molecules that comprise the atmosphere. The complete body of experimental evidence on a one-way attenuation through the total atmosphere, summarized in figure 4–28, is somewhat inconclusive. Its origin in molecular water vapor and O_2 absorption is well known; however, analytical schemes are needed to establish (by accurate correlations to meteorological variables) the utility of a particular remote-sensing method.

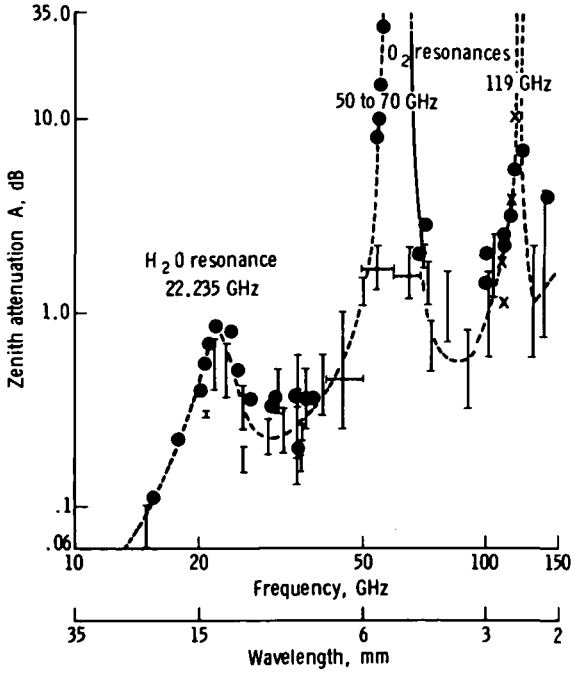

FIGURE 4–28.—Measured clear-sky zenith atmospheric attenuation in the range of 10 to 150 GHz (ref. 4–70).

The transfer properties of the total atmosphere are estimated from homogeneous gas conditions using numerical integration for modeled vertical pressure and temperature profiles. The H_2O and O_2 spectra for the homogeneous gas are discussed in the sections entitled "Water Vapor" and "Air" concerning their variability with frequency ν, dry air pressure p, water vapor pressure p_w, and temperature T as it occurs over the altitude range of $h=0$ to 90 km. Such a description of electromagnetic medium properties is, of course, fundamental to all active microwave remote-sensing schemes.

An emergent microwave signal is affected in amplitude, phase, and direction (refractive bending) by the intervening atmosphere; and the interaction can be a strong function of frequency. In addition, under special circumstances (O_2-microwave-spectrum (O_2-MS) Zeeman effect when $h>45$ km), a dependence on polarization and orientation can occur. Such behavior lends itself to active remote-sensing applications of atmospheric conditions, because the H_2O and O_2 resonance spectra are uniquely related to water vapor contents and to the dry airmass.

Gaseous transfer characteristics are expressed for homogeneous conditions in terms of attenuation coefficient k (in dB/km) and phase dispersion $\Delta\phi$ (in rad/km) by

$$k=0.1820\nu(N''_d+N''_w) \qquad (4\text{–}65)$$

and

$$\Delta\phi=0.02095\nu(\Delta N_d+\Delta N_w) \qquad (4\text{–}66)$$

where ν is the microwave frequency in GHz, and N''_d and N''_w are molecular extinction spectra of dry air (O_2 and ozone (O_3)) and of water vapor (H_2O and H_2OOH_2), and N_d and N_w are the corresponding dispersion spectra, all in units of ppm.

Cumulative transfer characteristics are evaluated by

$$\left.\begin{aligned} A &= \int_{h_i}^{h_f} k(l)\, dl \\ \Delta T &= \int_{h_i}^{h_f} \Delta\phi(l)\, dl \end{aligned}\right\} \qquad (4\text{–}67)$$

where A is zenith attenuation in decibels, ΔT is zenith dispersion in radians, dl is an increment of the ray path, h_i is the initial altitude, and h_f is the final altitude where $k(l)$ and $\Delta\phi(l)$ are essentially zero (h_f is approximately 90 km for O_2 and approximately 25 km for H_2O).

Water Vapor

Two rotational lines of the H_2O spectrum are centered at 22 and 183 GHz. The resonant part caused by these lines is evaluated by equations (4–65) and (4–66) using

$$\left.\begin{aligned} N''_w &= \sum_i (SF'')_i \\ \Delta N_{wc} &= \sum_i (SF')_i \end{aligned}\right\} \qquad (4\text{–}68)$$

where F is the pressure-broadened line, and the line strength S is given by

$$S = \frac{\nu}{\nu_0} S^\circ \left(\frac{300}{T}\right)^{3.5} p_{wc} \exp\left[w\left(1-\frac{300}{T}\right)\right] \qquad (4\text{–}69)$$

and for the intensity distribution of strongly air-broadened H_2O lines one assumes the shape

$$\left.\begin{aligned} F'_G &= \frac{2\nu_0(\nu_0^2-\nu^2)}{(\nu_0^2-\nu^2)^2+(2\nu\gamma_l)^2} \\ F''_G &= \frac{4\nu^2\gamma_l}{(\nu_0^2-\nu^2)^2+(2\nu\gamma_l)^2} \end{aligned}\right\} \qquad (4\text{–}70)$$

where the linewidth γ_l is given by

$$\gamma_l = \gamma^\circ\left[m_d\left(\frac{300}{T}\right)^{0.6} p + \left(\frac{300}{T}\right) p_{wc}\right] \qquad (4\text{–}71)$$

The line parameters given in table 4–VIII are at $T=300$ K (ref. 4–71).

The line spectrum of H_2O is not sufficient to account for water-vapor microwave attenuation away from the two line centers. A residual attenuation exists that can be postulated to consist of two parts: (1) the low-frequency wings of all H_2O rotational lines above 200 GHz, and (2) the microwave spectrum of a water vapor dimer H_2OOH_2.

The residual H_2O (monomer) attenuation can be estimated by

$$k_M \approx 4\times10^{-3}\, p_{wc}\left(\frac{\nu}{60}\right)^2\left(\frac{300}{T}\right)^{2.5} \qquad (4\text{–}72)$$

where k_M is in dB/km, p_{wc} is in torr, ν is in gigahertz, and T is in kelvin (e.g., when $p_{wc}=1$ torr, $T=280$ K, and $\nu=60$ GHz, then $k_M \approx 5\times10^{-3}$ dB/km).

The theory of a dimer attenuation k_D was treated in detail by Poon (ref. 4–72). The theoretical findings between 10 and 100 GHz can be roughly expressed by

$$k_D \approx 0.2\times10^{-3}\, p_{wc}^2\left(\frac{\nu}{60}\right)^{2.4}\left(\frac{300}{T}\right)^{17} \qquad (4\text{–}73)$$

(e.g., when $p_{wc}=10$ torr, $T=280$ K, and $\nu=60$ GHz, then $k_D \approx 65\times10^{-3}$ dB/km). Sketchy experimental evidence exists to somewhat support equations (4–72) and (4–73); however, much more experimental data need to be

TABLE 4–VIII.—*Line Spectrum Parameters at T=300 K for H_2O at 22 and 183 GHz*

Label	Individual lines of the H_2O microwave spectrum	
	1	2
Center frequency ν_0, GHz	22.23515	183.31012
Strength parameter S°, Hz/torr	[a] 13.9	[a] 322.0
Temperature exponent w, units	2.14	.653
Width (H_2O) γ°, MHz/torr	[a] 18.0	[a] 19
Broadening effect (air) m_d, units	.209	.21

[a] Unit of measurement fixed by the related equation.

gathered at different frequencies, temperatures, and close-to-saturation pressures.

The resonance dispersion ΔN_w offers a concept to measure the variability of atmospheric water vapor. The differential phase delay between two phase-coherent signals with frequencies on either side of the molecular resonance is a measure of the total amount of water vapor along the path. Such dual-frequency signals could be transmitted from a geostationary satellite and received by many ground stations. The technique has been investigated for line-of-sight ground-level paths (refs. 4–73 and 4–74). The integrated resonance dispersion for a vertical (zenith) path (fig. 4–29) provides some quantitative data. The calculation was based on equations (4–66), (4–67) (where $\Delta L = \Delta T c/2\pi\nu$), and (4–68) to 4–71). For the frequency pair 25.2 and 19.2 GHz, one obtains a phase change of 0.41° (0.015 mm/torr), which is sufficiently linear with each torr of ground-level water-vapor pressure.

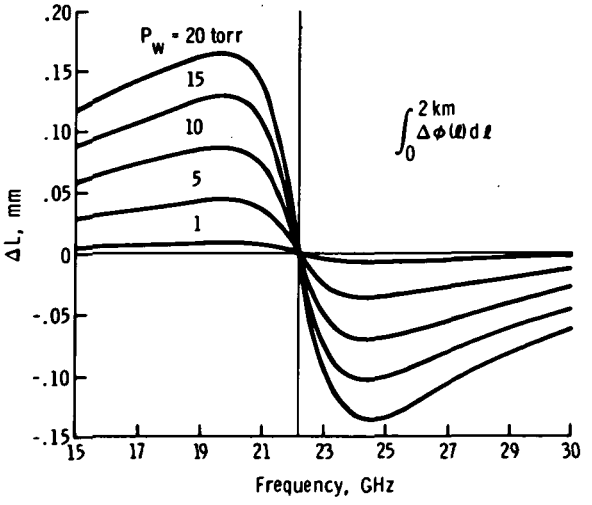

FIGURE 4–29.—Integrated resonance dispersion due to 22-GHz water-vapor line for vertical path through model atmosphere; p_w is water-vapor pressure at ground level (ref. 4–71). The model atmosphere was $p_0=760$ torr, $T_0=290$ K, and $p_w=1$ to 20 torr for ground-level conditions; exponential water-vapor distribution with 2.5-km scale height; $T=T_0-6.5h$ (km) and $p=p_0(T/T_0)^{5.53}$ for $h \leq 10$ km; $T=225$ K and $p=155\exp(-0.015)$ for $h > 10$ km.

The much stronger 183-GHz line, for a signal pair 187 and 179 GHz, yields a differential phase delay of approximately 50° per torr of ground-level water vapor; but it is associated with higher attenuation (approximately 15 dB).

Air

For all atmospheric transmission problems, it is sufficient to consider i less than or equal to 44 individual lines of the O_2-MS. Of these, 43 lines are centered around 60 GHz and 1 line at 119 GHz. Propagation parameters are evaluated using the following expressions for equations (4–65) and (4–66):

$$\left.\begin{aligned} N_d'' &= \sum_i (SF'')_i \\ \Delta N_d &= \sum_i (SF')_i \end{aligned}\right\} \qquad (4\text{–}74)$$

where N_d'' and ΔN_d are in ppm.

Each line strength is given in air by

$$S_i = 0.2090 \frac{\nu}{\nu_0^i} p\,[S^\circ \psi(T)]_i \qquad (4\text{–}75)$$

where S_i is in hertz and the temperature function (relative to $T_0=300$ K) is

$$\psi(T) = \left(\frac{300^3}{T}\right) \exp\left[-6.895\times10^{-3} N(N+1)\left(\frac{300}{T}-1\right)\right] \qquad (4\text{–}76)$$

where N is a quantum number.

Each pressure-broadened ($p \approx 1$ to 800 torr) line is described by the Lorentzian shape

$$\left.\begin{aligned} F' &= \frac{z}{\gamma_l(1+z^2)} \\ F'' &= \frac{1}{\gamma_l(1+z^2)} \end{aligned}\right\} \qquad (4\text{–}77)$$

where $z=(\nu_0^i-\nu)/\gamma_{l_i}$ is a dimensionless frequency.

The pressure-broadened linewidth (in megahertz) is

$$\gamma_{l_i}(p) = m_a(\gamma^\circ p - \xi p^2 + \cdots)\left(\frac{300}{T}\right)^{0.85} + \gamma^\circ m_w \frac{300}{T} p_w \quad (4\text{–}78)$$

where $m_a = 0.93$ and $m_w = 1.25$ are the broadening efficiencies in air and water vapor, respectively, and ξ (approximately equal to 0.0016 MHz/torr^2) is an empirical overlap coefficient (ref. 4–63). Table 4–IX

TABLE 4–IX.—*Spectroscopic Parameters of O_2 Microwave Line Spectrum*

O_2 line	Center frequency ν_0, GHz	Quantum number N		Strength S°, Hz/torr[a]	Width γ°, MHz/torr[a]	Remarks
		+	−			
1.....	48.942 4	.....	43^-	0.000 024	1.79	
	49.451 4	.....	41^-	.000 073	1.79	
	49.961 8	.....	39^-	.000 216	1.79	
	50.473 6	.....	37^-	.000 598	1.79	
5.....	50.987 3	.....	35^-	.001 564	1.79	
	51.503 02	.....	33^-	.003 860	1.79	
	52.021 17	.....	31^-	.008 985	1.79	
	52.542 23	.....	29^-	.019 707	1.79	
	53.066 80	.....	27^-	.040 717	1.79	
10.....	53.595 68	.....	25^-	.079 186	1.79	
	54.129 96	.....	23^-	.144 84	1.79	
	54.671 145 (20)	.....	21^-	.248 87	1.79	
	55.221 372 (20)	.....	19^-	.401 19	1.79	
	55.783 819 (20)	.....	17^-	.605 61	1.79	
15.....	56.264 778 (10)	1^+	.....	.348 69	2.26	Doublet
	56.363 393 (20)	.....	15^-	.853 87	1.79	98.62
	56.986 180 (20)	.....	13^-	1.120 4	1.79	
	57.612 49	.....	11^-	1.359 5	1.79	
	58.323 885 (10)	.....	9^-	1.515 0	1.79	Doublet
20.....	58.446 580 (10)	3^+	.....	.925 05	1.89	122.72
	59.164 215 (10)	.....	7^-	1.526 3	1.79	
	59.590 978 (10)	5^+	.....	1.341 0	1.81	
	60.306 044 (10)	.....	5^-	1.348 7	1.81	Doublet
	60.434 776 (10)	7^+	.....	1.562 6	1.79	128.74
25.....	61.150 565 (5)	9^+	.....	1.589 9	1.79	
	61.800 169 (10)	11^+	.....	1.458 8	1.79	
	62.411 223 (10)	13^+	.....	1.227 2	1.79	Doublet
	62.486 255 (10)	.....	3^-	.963 36	1.89	75.03
	62.998 00	15^+	.....	.954 01	1.79	
30.....	63.568 520 (10)	17^+	.....	.689 76	1.79	
	64.127 777 (20)	19^+	.....	.465 60	1.79	
	64.678 92	21^+	.....	.294 21	1.79	
	65.224 120 (20)	23^+	.....	.174 37	1.79	
	65.764 744 (20)	25^+	.....	.097 074	1.79	
35.....	66.302 06	27^+	.....	.050 820	1.79	
	66.836 77	29^+	.....	.025 041	1.79	
	67.369 51	31^+	.....	.011 621	1.79	
	67.900 73	33^+	.....	.005 083	1.79	
	68.430 8	35^+	.....	.002 096	1.79	
40.....	68.960 1	37^+	.....	.000 815	1.79	
	69.488 7	39^+	.....	.000 299	1.79	
	70.016 9	41^+	.....	.000 104	1.79	
	70.544 9	43^+	.....	.000 034	1.79	
44.....	118.759 343 (10)	.....	1^-	.597 25	2.10	Isolated line

[a] Relative to $T_0 = 300$ K.

lists the parameters for 44 lines labeled by line number or the quantum number $N^{\pm}$ (where ν_0 is center frequency, $S°$ is strength, and $\gamma°$ is width).

Transfer properties of homogeneous dry air.—The clean, dry atmosphere sustains a constant mixing ratio up to $h \leq 80$ km for all gases that might have a measurable influence on microwave transfer properties. An exception is ozone. The stronger lines of ozone in the microwave part of the spectrum are listed in table 4–X. A maximum zenith attenuation between 0.16 and 0.75 dB to ground level and a half-linewidth of approximately 30 MHz for an observation platform at $h=$ 12 km gives these lines some potential for the remote sensing of the atmospheric ozone content (refs. 4–75 and 4–76). However, the much stronger effects as a result of O_2 shall be emphasized here. Attenuation (eq. (4–65)) and dispersion (eq. (4–66)) related to the atmospheric O_2-MS are calculated using equations (4–74) to (4–78). The dependences on temperature and pressure follow from equations (4–75), (4–76), and (4–78). Results can be categorized as continuum, line, double-line (doublet), and line-Zeeman spectra in terms of altitude h increases.

1. Altitude $h<10$ km: All lines, except one at 119 GHz, are merged into a continuum spectrum under the influence of pressure broadening. Nonlinear (with respect to pressure) overlap effects are taken into account

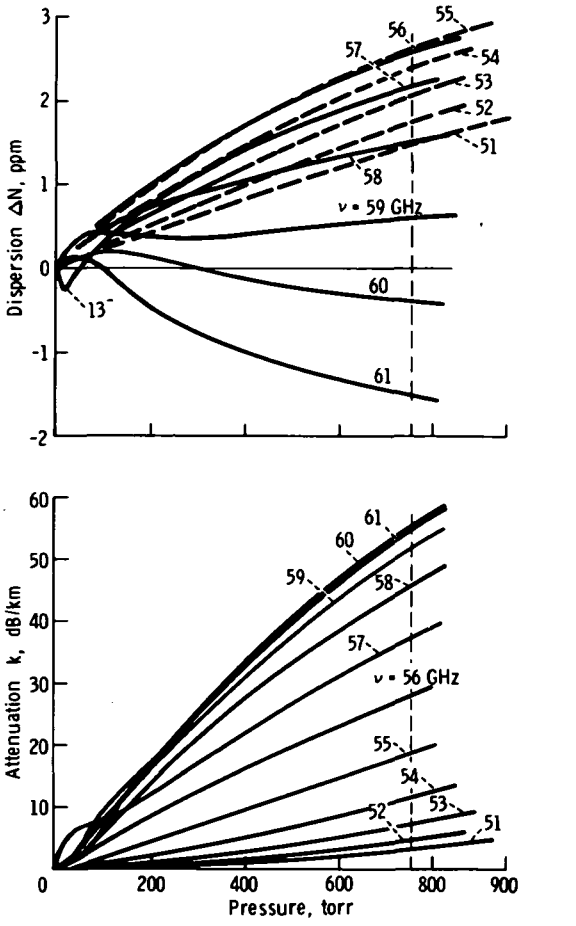

FIGURE 4–30.—Pressure profiles of the O_2 microwave continuum spectrum between 51 and 61 GHz at $T=300$ K. For dry air, multiply vertical scales (k and ΔN) by the factor 0.225. Simulated altitude range $h \approx 0$ to 20 km.

TABLE 4–X.—*Stronger Spectral Lines of Ozone in the 10- to 150-GHz Frequency Band* [a]

Center frequency, GHz	Maximum absorption of pure gas, dB/km [b]	Zenith absorption (maximum), dB [c]
96.2288	426	0.16
101.7368	803	.3
110.835	1230	.4
124.086	1750	.5
125.389	1030	
136.883	300	
142.172	2330	.75

[a] Data from refs. 4–75 and 4–76.

[b] Relative to $T_0=300$ K.

[c] Calculated for U.S. Standard Atmosphere (1962) (ref. 4–77) and daytime ozone distribution (maximum of 5×10^{13} molecules/cm^3 at $h=20$ km).

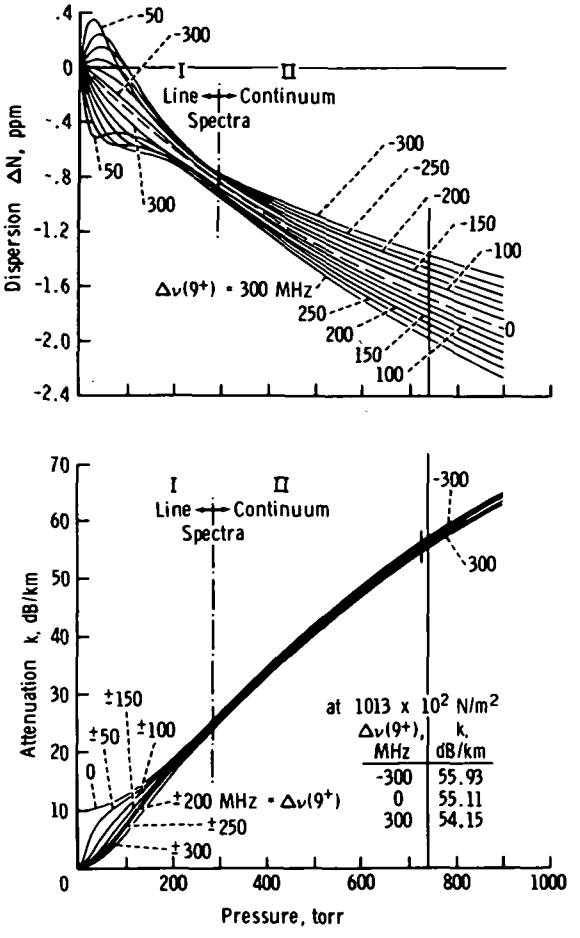

FIGURE 4–31.—Pressure profiles of the O_2 microwave spectrum in the vicinity ($\Delta\nu=\nu-\nu_0$) of the 9⁺ line ($\nu_0=61.1506$ GHz). For dry air, multiply vertical scales by 0.225. Simulated altitude range $h \approx 0$ to 20 km.

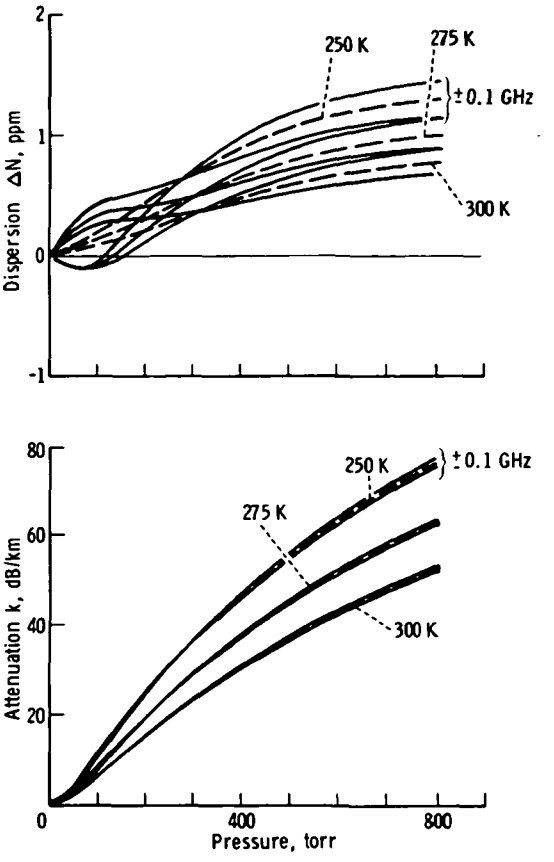

FIGURE 4–32.—Pressure profiles of the O_2 microwave continuum spectrum for $T=250$ to 300 K. The differential pressure sensitivity for $\nu\pm0.1$ GHz (58.8 ±0.1 GHz) is shown. For dry air, multiply vertical scales by 0.225. Simulated altitude range $h \approx 0$ to 20 km (ref. 4–78).

by the empirical parameter η. The results are given in figures 4–30, 4–31, and 4–32. The conversion factor from O_2 to air intensity (0.225) was experimentally verified. The attenuation can be approximated by a power-law form

$$k=\frac{Cp^{x(\nu)}T^{y(\nu)}}{1+\left(\frac{\nu_c-\nu}{\gamma_c}\right)^2} \qquad (4\text{–}79)$$

where C is a constant.

The pressure dependence on h is governed by the hydrostatic equation

$$p(h)=p_0e^{-h/H} \qquad (4\text{–}80)$$

where p_0 is the surface pressure, and $H=0.0293T(h)$ is the pressure scale height. An average atmospheric temperature $\bar{T}(h)=239$ K yields $H=7.0$ km (ref. 4–72). The vertical temperature profile, however, is not given by any simple physical model for $h<80$ km and must be taken from tables for model atmospheres.

2. Altitude $h>30$ km: An isolated line spectrum is displayed. The summation in equation (4–74) can be reduced to the response of a single line plus an unstructured background term. An example displays pressure profiles in the vicinity of the 9⁺ line (fig. 4–31). The response of the four O_2-MS doublets falls in the same category. The

normal line spacing is roughly 500 MHz, whereas the doublets are separated only by approximately 100 MHz. The example given in figure 4–33 shows the more complicated pressure dependence of k and ΔN. The doublet is suited to experimentally study the overlap effects (whereby the problem is reduced to two lines instead of $i=1$ to 43).

3. Altitude $h>45$ km: Zeeman-splitting of each O_2-MS line in the Earth magnetic field becomes noticeable and causes anisotropic, polarization-dependent transfer properties

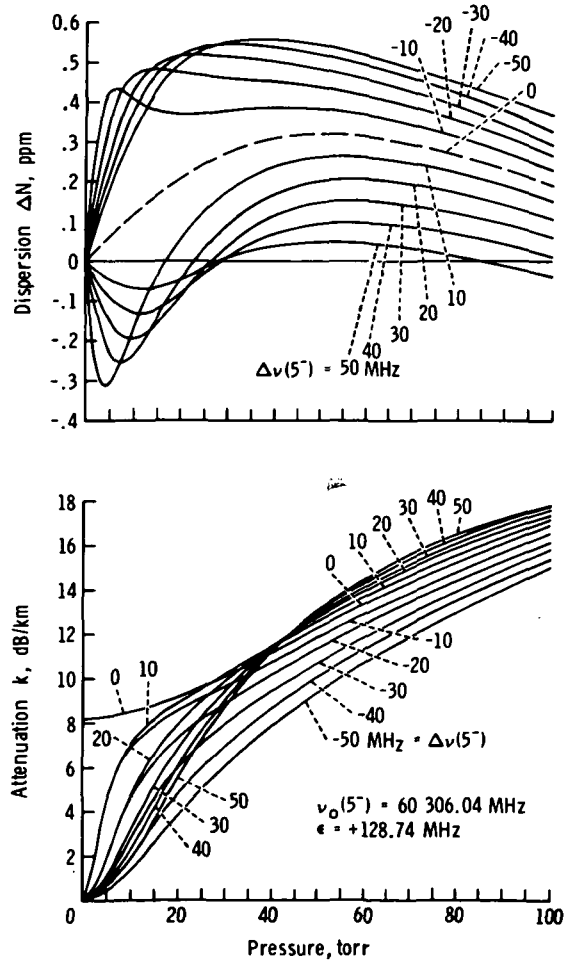

FIGURE 4–33.—Pressure profiles of the O_2 microwave line spectrum (300 K) in the vicinity ($\Delta\nu=\nu-\nu_0$) of the $5^-/7^+$ doublet (the separation to ν_0 (7^+) is given by ϵ). For dry air, multiply vertical scales by 0.225. Simulated altitude range $h\approx 15$ to 40 km.

(ref. 4–63). At these altitudes, the lines are only a few megahertz wide, although individual Zeeman components are not resolved. Each O_2-MS line assumes a constant width under the influence of a magnetic field and rapidly approaches zero intensity as the pressure drops below 1 torr. An example (fig. 4–34) treats the case of the 1^+ line, which splits into two σ-components when the magnetic-field vector of linearly polarized radiation is assumed to be perpendicular to the direction of the Earth magnetic-field strength in the plane perpendicular to the propagation direction.

For remote-sensing applications, it is important to know the frequency, pressure, and temperature sensitivities of O_2-MS transfer characteristics for a given condition. An example is given in figure 4–32.

Transfer properties of the total dry airmass.—The total atmospheric O_2-MS contains all the cases discussed in the previous section concerning transfer properties of homogeneous dry air (oxygen). The complexity of the problem is underlined by the various homogeneous gas conditions presented in figures 4–30 to 4–34. A solution of equation (4–67) was approximated by assuming a spherically stratified atmosphere with $i=151$ homogeneous slabs for $h=0$ to 90 km and a numerical integration based on Simpson's rule as follows:

$$\left.\begin{aligned} A &= 0.5\sum (k_i+k_{i+1})\,\Delta l_i(\theta) \\ \Delta T &= 0.5\sum (\Delta\phi_i+\Delta\phi_{i+1})\,\Delta l_i(\theta) \end{aligned}\right\} \qquad (4\text{–}81)$$

where A is in decibels and ΔT is in radians. The slant-path-length increments Δl_i are calculated along a straight-line path using an algorithm based on the starting angle against zenith θ (ref. 4–63). The results for three different initial altitudes ($h_i=h_l=0$, 10, and 20 km) are shown in figure 4–35.

Molecular emission produces an antenna noise temperature proportional to the integral over the attenuation rate and temperature distribution along the path at which the antenna is looking. This is the basis for the

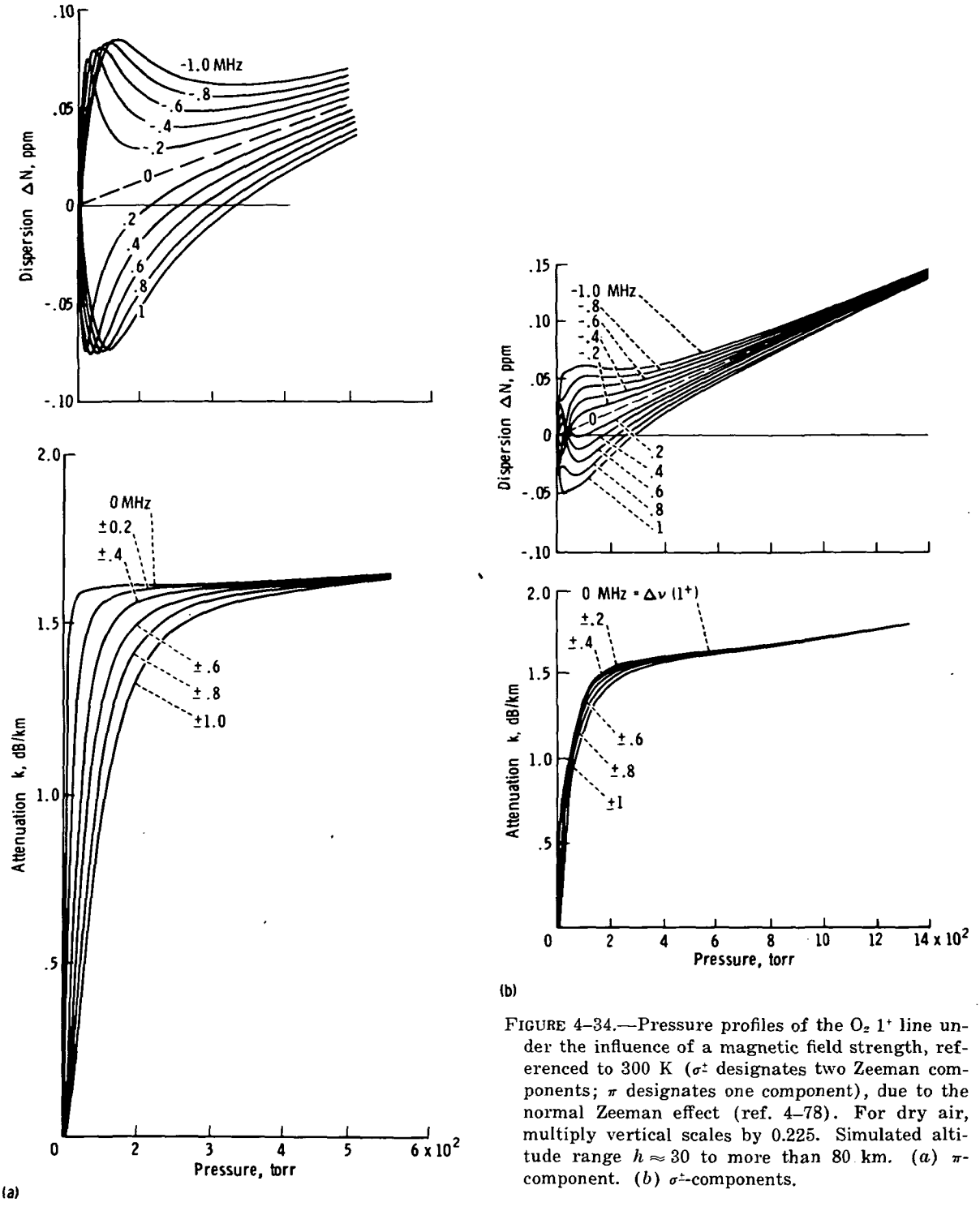

FIGURE 4–34.—Pressure profiles of the O_2 1^+ line under the influence of a magnetic field strength, referenced to 300 K ($\sigma^{\pm}$ designates two Zeeman components; π designates one component), due to the normal Zeeman effect (ref. 4–78). For dry air, multiply vertical scales by 0.225. Simulated altitude range $h \approx 30$ to more than 80 km. (*a*) π-component. (*b*) $\sigma^{\pm}$-components.

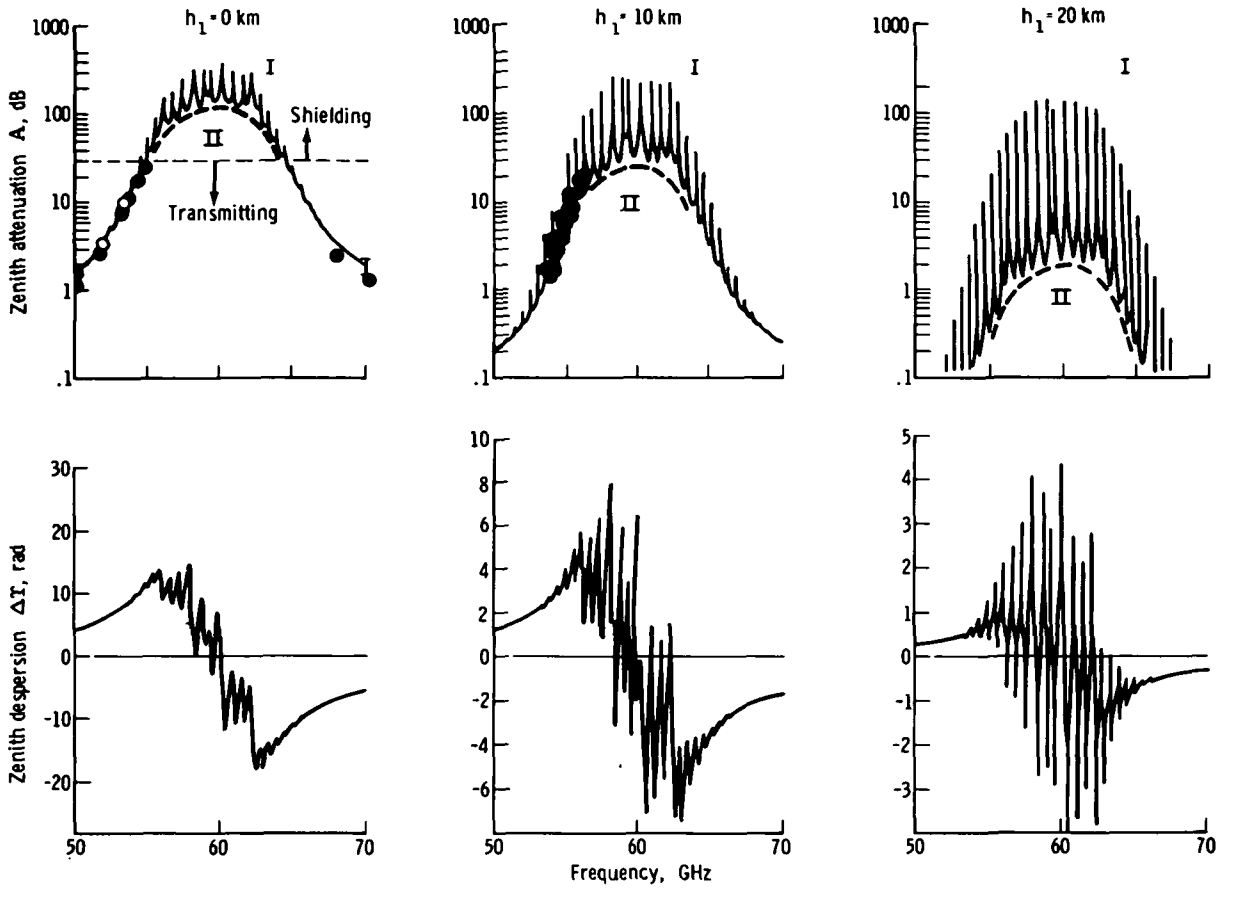

FIGURE 4–35.—One-way attenuation A and phase dispersion ΔT due to the O_2 microwave spectrum between 49 and 72 GHz for a zenith path through the U.S. Standard Atmosphere 1962 (ref. 4–77) from three different initial altitudes h_1 to outer space (I-line, II-continuum spectra). (For experimental points for $h_1=0$, see fig. 4–30.)

passive (radiometric) remote-sensing application to globally map vertical temperature structures from a satellite. In active systems, this atmospheric noise poses a problem because it sets an ultimate limit to the receiver sensitivity. Across the O_2-MS band, the noise temperature varies between 3 K ($A=0$ dB) and 300 K ($A>50$ dB), which is, however, still of no concern because mixer noise is considerably higher.

The resonance dispersion ΔN_d offers a concept to measure the variability of the dry airmass. The differential phase delay between two phase-coherent signals with frequencies on either side of the 60-GHz band is a measure of dry air conditions. The extreme values of O_2-MS zenith dispersion from $h=0$ to outer space (fig. 4–35) are shown in table 4–XI. The nondispersive delay $\Delta\tau$ caused by the vertical refractivity profile is approximately 7000 psec for a zenith path at 60 GHz. Moving the sensing frequency pair into the edges of the O_2-MS band increasingly favors the gas mass at the lower altitudes.

The same differential principle applies to attenuation in the semitransparent O_2-MS portions ($55<\nu<65$ GHz). By defining an equivalent altitude h_k for the zenith O_2-MS attenuation A (fig. 4–35) (where the homogeneous ground-level attenuation coefficient k (fig. 4–36) equals A), one obtains $h_k=$ 18 km (at a maximum of 60.4 GHz) and

TABLE 4–XI.—*Extreme Values of O_2-MS Zenith Dispersion*

Frequency ν, GHz	Zenith dispersion ΔT, rad	$\Delta L=(\Delta Tc)/(2\pi\nu)$, mm	$\Delta\tau=\Delta T/(2\pi\nu)$, psec
58.3	+15	+12	+40
	33	26	85
62.6	−18	−14	−45

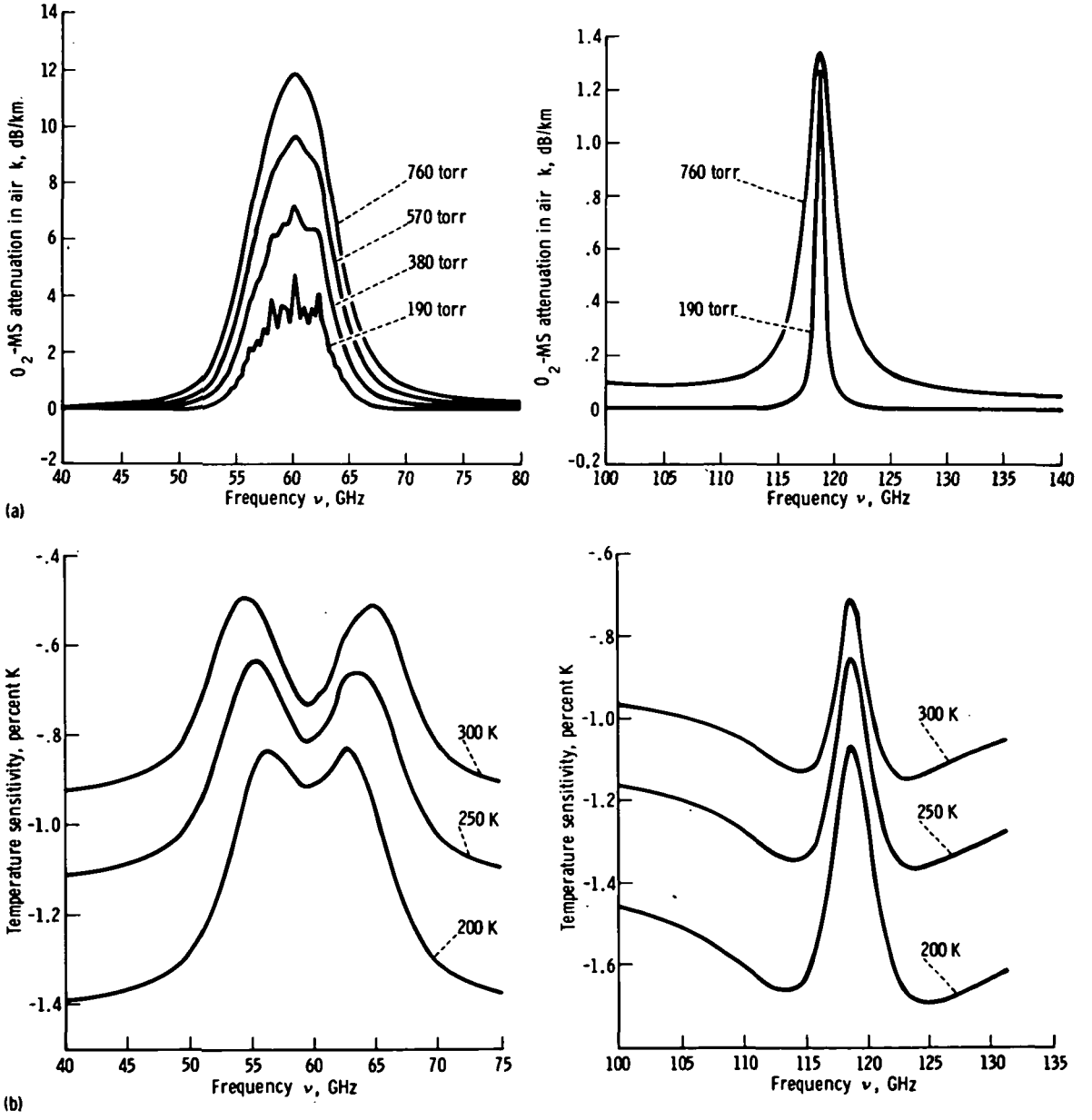

FIGURE 4–36.—The O_2 microwave spectrum attenuation and its pressure and temperature sensitivities to various atmospheric conditions over the 40- to 140-GHz band (ref. 4–78). (*a*) Attenuation in air k compared with frequency $\nu(T=300$ K). (*b*) Temperature sensitivity compared with frequency $\nu(p=760$ torr).

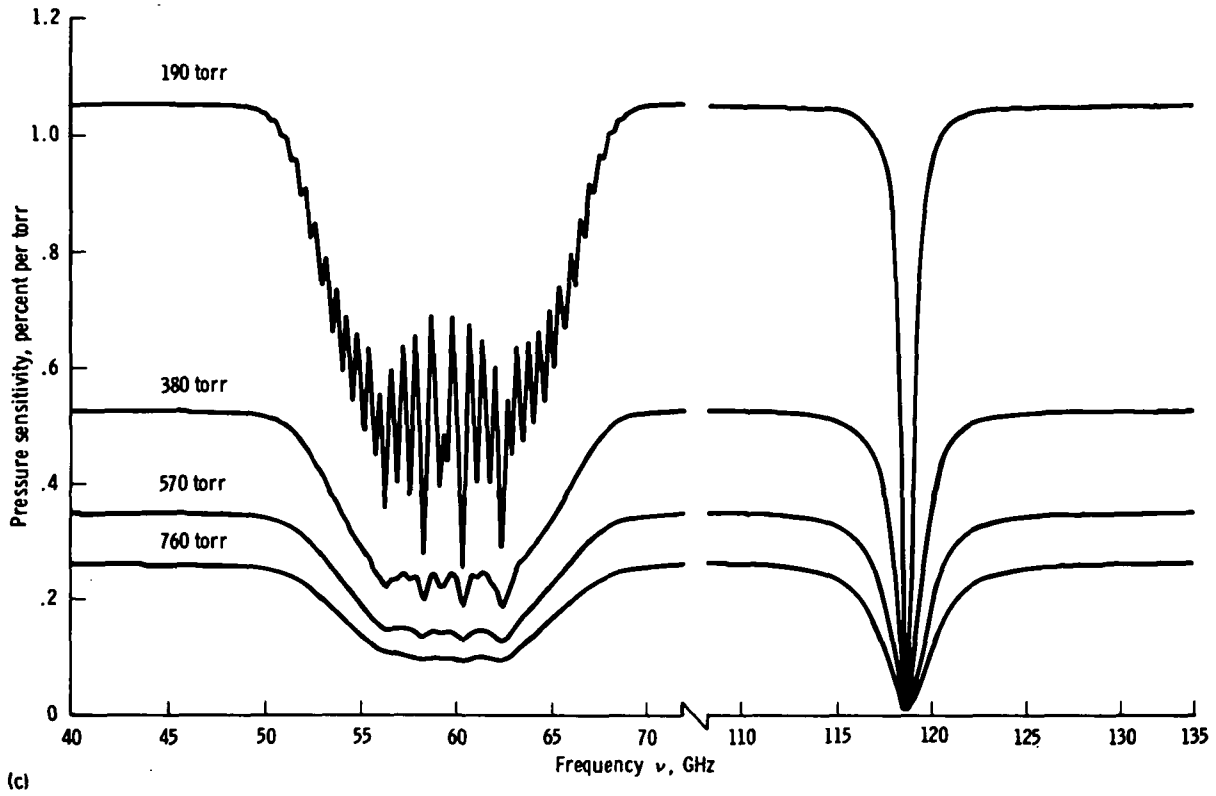

FIGURE 4–36 (concluded).—The O_2 microwave spectrum attenuation and its pressure and temperature sensitivities to various atmospheric conditions over the 40- to 140-GHz band (ref. 4–78). (*c*) Pressure sensitivity compared with frequency $\nu(T=300$ K).

$h_k=5$ km (for $50<\nu<55$ GHz and $66<\nu<72$ GHz).

A proposal has been made to measure surface pressure by a differential intensity measurement of two satellite-based radar signals reflected from the Earth surface (ocean), whereby one frequency lies in the semitransparent O_2-MS range and the other is remote from the O_2-MS in a transparent range. (See the section entitled "The Measurement of Surface Pressure From a Satellite by Active Microwave Techniques.") The calculations for the U.S. Standard Atmosphere, 1962 (ref. 4–77) yield the values of h_k given in the previous paragraph, which predict essentially constant opacity ($h_k=5$ km); hence, the attenuation response of the total airmass may be evaluated by equation (4–79). The values of x and y at a particular frequency (figs. 4–30 to 4–34) are the significant parameters for a radar sensing of surface pressure.

One can conceive possibilities for atmospheric research with a microwave system consisting of a transmitter on one spacecraft and a receiver on another. (See the section entitled "Applications of Bistatic Microwave Systems to Atmospheric Research.") Atmospheric occultation at frequencies in the two O_2-MS bands centered at 60 and 119 GHz can exploit the properties of individual O_2-MS lines when the closest approach to ground level is $h>15$ km. Two possible applications are:

1. The peak attenuation of the two $N=15^{\pm}$ lines (table 4–IX) is independent of temperature and thus a good indicator of stratospheric pressure (ref. 4–63).

2. The fact that the transfer characteristics in the vicinity of the $1^{\pm}$ lines (fig. 4–34) are dependent in the least complicated manner upon strength and orientation of the

Earth magnetic field suggests magnetometer applications.

Conclusions

Technically, there are several promising remote-sensing concepts that can benefit from or are affected by H_2O and O_2 spectroscopic transfer characteristics. The following research will provide a basis for the development of remote-sensing schemes operating in the 10- to 150-GHz frequency range:

1. The translation of molecular theory on millimeter wave properties of air into engineering terms.

2. The description of analytical schemes to predict propagation phenomena on the basis of meteorological variables, together with examples of unique atmospheric transfer properties.

Laboratory work is recommended to better define the spectroscopic parameters of atmospheric microwave transfer characteristics as a function of pressure, composition, temperature, and magnetic-field strength over the range of these variables encountered in the atmosphere.

REFERENCES

4–1. The Atmospheric Sciences and Man's Needs, Priorities for the Future. Printing and Publishing Office, National Academy of Sciences (Washington, D.C.), 1971.

4–2. Report of the Planning Conference on the First GARP Global Experiment. World Meteorological Organization and International Council of Scientific Unions (Geneva, Switzerland), Sept. 1972.

4–3. LIGDA, MYRON G. H.: Radar Storm Observation. Compendium Meteorology, Amer. Meteorol. Soc. (Boston, Mass.), 1951, pp. 1265–1282.

4–4. MARSHALL, J. S.; HITSCHFELD, WALTER; AND GUNN, K. L. S.: Advances in Radar Weather. Advances in Geophysics, vol. II, H. E. Landsberg, ed. Academic Press (New York), 1955, pp. 1–56.

4–5. VAN BLADEL, J.: Les Applications du Radar à L'Astronomie et à La Météorologie. Gauthier-Villars (Paris, France), 1955.

4–6. MARSHALL, J. S., AND GORDON, W. E.: Radiometeorology. Meteorol. Monogr., vol. 3, no. 14, July 1957, pp. 73–113.

4–7. BATTAN, LOUIS J.: Radar Meteorology. Univ. of Chicago Press, 1959.

4–8. ATLAS, DAVID: Advances in Radar Meteorology. Advances in Geophysics, vol. X, Academic Press (New York), 1964, pp. 317–478.

4–9. STEPANENKO, V. D.: Radar in Meteorology. Gidrometeoizdat (Leningrad), 1966. (Partial translation available from Joint Publications . Research Service, Washington, D.C.)

4–10. KOSTAREV, V. V.; CHERNIKOV, A. A.; AND SHUPYATSKII, A. B., eds.: Radar Meteorology. Translation of the 1968 Proceedings of the Third All-Union Conference. Israel Program for Sci. Transl., 1971. (Available as IPST 5809.)

4–11. BATTAN, LOUIS J.: Radar Observation of the Atmosphere. Univ. of Chicago Press, 1973.

4–12. STEPANENKO, V. D.: Radar in Meteorology. Second ed. Gidrometeoizdat (Leningrad), 1973.

4–13. SMITH, PAUL L., JR.; HARDY, KENNETH R.; AND GLOVER, KENNETH M.: Applications of Radar to Meteorological Operations and Research. Proc. IEEE, vol. 62, no. 6, June 1974, pp. 724–745.

4–14. LIGDA, M. G. H.: Middle Latitude Precipitation Patterns as Observed by Radar. Rep. 574 T, Dept. of Oceanography and Meteorology, Texas A. & M. Univ., Jan. 1957.

4–15. MCGREW, RUSSELL G.: Project D/RADEX (Digitized Radar Experiments). The 15th Radar Meteorology Conference, Amer. Meteorol. Soc. (Boston, Mass.), 1972, pp. 101–106.

4–16. OSTLUND, STELLAN SVEN: Computer Software for Rainfall Analyses and Echo Tracking of Digitized Radar Data. Tech. Memo. ERL WMPO–15, NOAA Environmental Research Labs. (Boulder, Colo.), 1974.

4–17. WEXLER, HARRY: Observing the Weather From a Satellite Vehicle. J. Brit. Interplanet. Soc., vol. 13, no. 5, Sept. 1954, pp. 269–276.

4–18. WIDGER, WILLIAM K., JR., AND TOUART, C. N.: Utilization of Satellite Observations in Weather Analysis and Forecasting. Amer. Meteorol. Soc. Bull., vol. 38, no. 9, Nov. 1957, pp. 521–533.

4–19. MOOK, CONRAD P., AND JOHNSON, DAVID S.: Proposed Weather Radar and Beacon System for Use With Meteorological Earth Satellites. IRE Third National Convention on Military Electronics (New York), 1959, pp. 206–209.

4–20. KATZENSTEIN, H., AND SULLIVAN, H.: A New

Principle for Satellite-Borne Meteorological Radar. Proceedings of the 8th Weather Radar Conference, Amer. Meteorol. Soc. (Boston, Mass.), 1960, pp. 505–515.

4–21. KEIGLER, J. E., AND KRAWITZ, L.: Weather Radar Observations From an Earth Satellite. J. Geophys. Res., vol. 65, no. 9, Sept. 1960, pp. 2793–2808.

4–22. DENNIS, ARNETT S.: Rainfall Determinations by Weather Radar on Meteorological Satellite Radar. NASA CR–50193, 1963.

4–23. DENNIS, ARNETT S.: Fundamental Limitations on Precipitation Observations From Satellites. NASA CR–52848, 1963.

4–24. Radar for Meteorology. Useful Applications of Earth-Oriented Satellites. Panel 4, App. G, NASA CR–101401, 1969, pp. 69–73.

4–25. KRISHNAMURTI, T. N.; KANAMITSU, M.; CESELSKI, B.; AND MATHUR, M. B.: Florida State University's Tropical Prediction Model. Tellus, vol. 25, no. 6, 1973, pp. 523–535.

4–26. KURIHARA, YOSHIO, AND TULEYA, ROBERT E.: Structure of a Tropical Cyclone Developed in a Three-Dimensional Numerical Simulation Model. J. Atmos. Sci., vol. 31, no. 4, May 1974, pp. 893–919.

4–27. MATHUR, MUKUT B.: Multiple-Grid Primitive Equation Model to Simulate the Development of an Asymmetric Hurricane. J. Atmos. Sci., vol. 31, no. 2, Mar. 1974, pp. 371–393.

4–28. MILLER, BANNER I.; CHASE, PETER P.; AND JARVINEN, BRIAN R.: Numerical Prediction of Tropical Weather Systems. Mon. Weather Rev., vol. 100, no. 12, Dec. 1972, pp. 825–835.

4–29. OOYAMA, KATSUYUKI: Numerical Simulation of the Life Cycle of Tropical Cyclones. J. Atmos. Sci., vol. 26, no. 1, Jan. 1969, pp. 3–40.

4–30. ROSENTHAL, STANLEY L.: Circularly Symmetric, Primitive Equation Model of Tropical Cyclone Development Containing an Explicit Water Vapor Cycle. Mon. Weather Rev., vol. 98, no. 9, Sept. 1970, pp. 643–663.

4–31. SUNDQVIST, HILDING: Numerical Simulation of the Development of Tropical Cyclones With a Ten-Level Model, pt. I. Tellus, vol. 22, no. 4, 1970, pp. 359–390.

4–32. ANTHES, RICHARD A.: Data Assimilation and Initialization of Hurricane Prediction Models. J. Atmos. Sci., vol. 31, no. 3, Apr. 1974, pp. 702–719.

4–33. TRACTON, M. S.: The Role of Cumulus Convection in the Development of Extra-Tropical Cyclones. Preprints, Eighth Conference Severe Local Storms, Amer. Meteorol. Soc. (Boston, Mass.), 1973, pp. 337–342.

4–34. ATLAS, D., AND ULBRICH, C. W.: The Use of Attenuation and Reflectivity for Improved Measurements of Water Content and Rainfall Rate. IUCRM—Colloquium on Fine Scale Structure of Precipitation and E.M. Propagation (Nice, France), Oct. 21, 1973.

4–35. ECCLES, P. J., AND ATLAS, D.: A New Method of Hail Detection by Dual-Wavelength Radar. The 14th Radar Meteorology Conference, Amer. Meteorol. Soc. (Boston, Mass.), 1970, pp. 1–6.

4–36. GOLDHIRSH, JULIUS, AND KATZ, ISADORE: Estimation of Raindrop Size Distribution Using Multiple Wavelength Radar Systems. Radio Sci., vol. 9, no. 4, Apr. 1974, pp. 439–446.

4–37. GUNN, K. L. S., AND EAST, T. W. R.: The Microwave Properties of Precipitation Particles. Quart. J. Roy. Meteorol. Soc., vol. 80, no. 346, Oct. 1954, pp. 522–545.

4–38. HADDOCK, F. T.: Scattering and Attenuation of Microwave Radiation Through Rain, Report of NRL Progress. Naval Research Laboratory (Washington, D.C.), June 1956, pp. 15–21.

4–39. MEDHURST, RICHARD G.: Rainfall Attenuation of Centimeter Waves: Comparison of Theory and Measurement. IEEE Trans. Antennas Propagat., vol. AP–13, no. 1, Jan. 1965, pp. 550–564.

4–40. WEXLER, RAYMOND, AND ATLAS, DAVID: Radar Reflectivity and Attenuation of Rain. J. Appl. Meteorol., vol. 2, no. 2, Apr. 1963, pp. 276–280.

4–41. MARSHALL, J. S., AND PALMER, W. MCK.: The Distribution of Raindrops With Size. J. Meteorol., vol. 5, no. 4, Aug. 1948, pp. 165–166.

4–42. MITCHELL, R. L.: Radar Meteorology at Millimeter Wavelengths. Rep. SSD TR–66–117, U.S. Air Force, Space Systems Division, 1966.

4–43. ATLAS, D., AND CHMELA, A. C.: Physical-Synoptic Variations of Drop-Size Parameters. Proceedings of the 6th Weather Radar Conference, Amer. Meteorol. Soc. (Boston, Mass.), 1957, pp. 21–29.

4–44. HARDY, WALTER N.; GRAY, KENNETH W.; AND LOVE, A. W.: An S-Band Radiometer Design With High Absolute Precision. IEEE Trans. Microwave Theory Tech., vol. MTT–22, no. 4, Apr. 1974, pp. 382–390.

4–45. MOORE, RICHARD K.: Ground Echo. Radar Handbook, ch. 25, Merrill I. Skolnik, ed., McGraw-Hill Book Co., 1970.

4–46. RUCK, GEORGE T.; BARRICK, DONALD E.; STUART, WILLIAM D.; AND KRICHBAUM, CLARENCE K.: Radar Cross Section Handbook, vol. I, George T. Ruck, ed., Plenum Press, 1970.

4–47. SPILHAUS, A. F.: Raindrop Size, Shape, and Falling Speed. J. Meteorol., vol. 5, no. 3, June 1948, pp. 108–110.

4–48. MCCORMICK, G. C., AND HENDRY, A.: The Study of Precipitation Backscatter at 1.8 cm With a Polarization Diversity Radar. The 14th Radar Meteorology Conference, Amer. Meteorol. Soc. (Boston, Mass.), 1970, pp. 225–230.

4–49. HENDRY, A., AND MCCORMICK, G. C.: Deterioration of Circular-Polarization Clutter Cancellation in Anisotropic Precipitation Media. Electron. Lett., vol. 10, no. 10, May 1974, pp. 165–166.

4–50. JONES, R. F.: Size-Distribution of Ice Crystals in Cumulonimbus Clouds. Quart. J. Roy. Meteorol. Soc., vol. 86, no. 368, Apr. 1960, pp. 187–194.

4–51. LHERMITTE, ROGER M.: Atmospheric Probing by Doppler Radar. Atmospheric Exploration by Remote Probes, vol. 2, National Academy of Sciences, 1968, pp. 253–285.

4–52. LHERMITTE, ROGER M.: Dual-Doppler Radar Observation of Convective Storm Circulation. The 14th Radar Meteorology Conference, Amer. Meteorol. Soc. (Boston, Mass.), 1970.

4–53. LHERMITTE, ROGER M.: Kinematics of Sea Breeze Storms. Geophys. Res. Newsletter, vol. 1, no. 3, July 1974, pp. 123–125.

4–54. LHERMITTE, ROGER M.: Real Time Monitoring of Convective Storm Processes by Dual Doppler Radar. Atmospheric Technology, no. 6, National Center for Atmospheric Research (Boulder, Colo.), 1975.

4–55. DONALDSON, RALPH J., JR.: Vortex Signature Recognition by a Doppler Radar. J. Appl. Meteorol., vol. 9, no. 4, Aug. 1970, pp. 661–670.

4–56. DOVIAK, R. F.; SIRMANS, D.; AND LEMMON, L.: Doppler Velocity and Reflectivity Structure Observed Within Tornadic Storms. Journal de Recherches Atmospheriques, May 1974.

4–57. JOSEPH, A. S.: Heterojunction PbSnTe Detectors Solve IR System Problems. Electro-Opt. Syst. Design, vol. 5, Oct. 1973, pp. 24–29.

4–58. RENSCH, D. B., AND LONG, R. K.: Comparative Studies of Extinction and Backscattering by Aerosols, Fog, and Rain at 10.6μ and 0.63μ. Appl. Opt., vol. 9, no. 7, July 1970, pp. 1563–1573.

4–59. ELTERMAN, LOUIS; TOOLIN, ROBERT B.; AND ESSEX, JOHN D.: Stratospheric Aerosol Measurements With Implications for Global Climate. Appl. Opt., vol. 12, no. 2, Feb. 1973, pp. 330–337.

4–60. MCCOY, JOHN H.; RENSCH, DAVID B.; AND LONG, RONALD K.: Water Vapor Continuum Absorption of Carbon Dioxide Laser Radiation Near 10μ. Appl. Opt., vol. 8, no. 7, Dec. 1968, pp. 1471–1478.

4–61. CHU, T. S., AND HOGG, D. C.: Effects of Precipitation on Propagation at 0.63, 3.5, and 10.6 Microns. Bell Syst. Tech. J., vol. 47, no. 5, May–June 1968, pp. 723–759.

4–62. The Planning of the First GARP Global Experiment. GARP Publ. no. 3, World Meteorological Organization (Geneva, Switzerland), 1969.

4–63. LIEBE, H. J., AND WELCH, W. M.: Molecular Attenuation and Phase Dispersion Between 40 and 140 GHz for Path Models From Different Altitudes. NASA CR–138495, 1973.

4–64. KRISHEN, K.: Mathematical Model for the Relationship of Radar Backscattering Cross Sections With Ocean Scene and Wind Velocity. Proceedings of the Seventh International Symposium on Remote Sensing of Environment, vol. III, Univ. of Michigan, May 1971, pp. 1861–1877.

4–65. SINGER, S. FRED: Measurement of Atmospheric Surface Pressure With a Satellite-Borne Laser. Appl. Opt., vol. 7, no. 6, June 1968, pp. 1125–1127.

4–66. WATTS, B. E.; HOWARD, A. M.; AND GIBBONS, G.: Double-Drift Millimetre-Wave Impatt Diodes Prepared by Epitaxial Growth. Electron. Lett., vol. 9, no. 8/9, May 1973, pp. 183–184.

4–67. BENOIT, ANDRE: Signal Attenuation Due to Neutral Oxygen and Water Vapor, Rain and Clouds. Microwave J., vol. 11, Nov. 1968, pp. 73–80.

4–68. SASAKI, Y.: An Objective Analysis Based on the Variational Method. J. Meteorol. Soc. Japan, ser. 2, vol. 36, no. 3, June 1958, pp. 77–88.

4–69. GHIL, M.: On Balance and Initiatization—Obtaining Data for Solving Initial-and-Boundary-Value Problems for Equations of Large Scale Dynamic Meteorology. Rep. IMM 400, Courant Inst. of Mathematical Sciences, New York Univ., Dec. 1973.

4–70. THOMPSON, W. I., III: Atmospheric Transmission Handbook. NASA CR–117173, 1971.

4–71. LIEBE, H. J.: Calculated Tropospheric Dispersion and Absorption Due to the 22-GHz Water Vapor Line. IEEE Trans. Antennas Propagat., vol. AP–17, no. 5, Sept. 1969, pp. 621–627.

4–72. POON, R. K.: Atmospheric Opacity Near Half Centimeter Wavelength. Ph.D. dissertation, Massachusetts Inst. of Technology, May 1974.

4–73. SULLIVAN, JOHN F., AND RICHARDSON, HAROLD

M.: Propagation of 15.6–31.2 GHz and 45–90 GHz Coherent Signal Pairs. AGARD Conf. Proc. No. 107 on Telecommunications Aspects on Frequencies Between 10 and 100 GHz, Sept. 1972, pp. 10/1–10/11.

4–74. THOMPSON, M. C.; WOOD, L. E.; AND JONES, H. B.: Phase and Fading Characteristics in the 10 to 40 GHz Band. Dept. of Commerce, Office of Telecommunications, Institute for Telecommunications Sciences Tech. Memo. prepared for NASA–LRC (Contract No. L–48, 854), Oct. 1972.

4–75. WATERS, J. W., AND PETRO, L. D.: Microwave Spectrum of Atmospheric Ozone. MIT–QPR No. 96, Research Laboratory of Electronics, Massachusetts Inst. of Technology, Jan. 1970, pp. 42–48.

4–76. WATERS, J.: Ground-Based Microwave Spectroscopic Probing of the Strato- and Mesosphere. Ph.D. dissertation, Massachusetts Inst. of Technology, Dec. 1970.

4–77. U.S. Standard Atmosphere, 1962. Superintendent of Documents, U.S. Government Printing Office (Washington, D.C.), 1962.

4–78. LIEBE, H. J.: Studies of Oxygen and Water Vapor Microwave Spectra Under Simulated Atmospheric Conditions. Dept. of Commerce, Office of Telecommunications, Institute for Telecommunications Sciences (Boulder, Colo.), 1974.

APPENDIX 4A

This appendix is based on a translation of section 9.6, entitled "Features and Effectiveness of the Detection of Clouds and Rain With Pulse Radar From Satellites," from Radar in Meteorology by V. D. Stepanenko (ref. 4–12).

UTILIZATION OF SCANNING BEAM RADAR

The capability of detecting a meteorological target with radar increases with the increase in transmitter power P_t and receiver sensitivity P_{min}. When interfering echo signals from the surface of the Earth are absent (as will often be the case for scanning-pencil beams produced by ground-based radar used for detection of the upper portion of clouds and rain), the required values of the radar parameters may be found from the basic radar equation.

When using radar in satellites, the widths of the radiation pattern $\theta_1\theta_2$ cannot be arbitrary; rather, they must be selected to insure a total angle of scan that will cover the Earth without any gaps. The radar-detection range depends on the orbit height and the given width of the region of coverage. The minimum height of the orbit is about 200 km; consequently, it is also the minimum detection range. This appears to be a disadvantage that is absent with ground-based radar; and, in the case of satellite-borne instruments, the limitations imposed by the present level of radar development prohibit the detection of weakly reflecting targets.

However, one of the advantages of using radar aboard satellites is the significantly large value of the beam-filling factor k_z at great distances in comparison with that for Earth-based radar (fig. 4A–1). In the latter case, the maximum range of showers and thunderstorms (the vertical dimensions of which are approximately 10 km) does not exceed 300 to 350 km. At greater ranges, they are located beneath the Earth-based antenna beam ($k_z=0$). At smaller ranges (200 to 250 km), the filling factor is only approximately several hundredths, even for narrow beamwidth ($\theta\approx1°$). In the same conditions, it is possible for satellite radar to have values of k_z of greater magnitude. This is readily shown from figure 4A–1. The magnitude of the beam filling factor at the Earth surface is

$$k_z' = \frac{h'}{\theta_2(H+h-h')\ \operatorname{cotan} A} \quad (4A\text{–}1)$$

After the pulse reaches the Earth surface

$$k_z'' = \frac{h}{(H\ \operatorname{cotan} A + B\epsilon' \cos^2 A)\,\theta_2} \quad (4A\text{–}2)$$

with

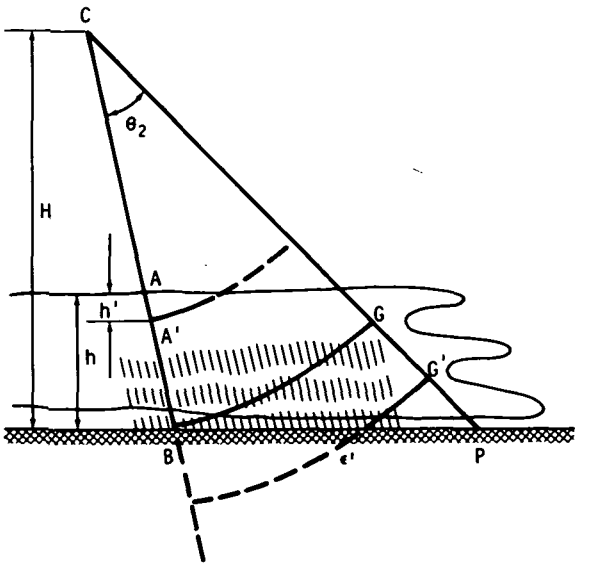

FIGURE 4A-1.—Geometry for computing the filling factor for satellite radar.

$$CG \geq \frac{H-h}{\sin(A-\theta_2)} \qquad (4A\text{–}3)$$

and

$$k_z'' = \frac{(BP - B\epsilon')\sin A}{\left(\frac{H}{\sin A} + \frac{B\epsilon'}{\cos A}\right)\theta_2} \qquad (4A\text{–}4)$$

Another advantage of using radar in a satellite is the possibility of detecting clouds and rain from overhead (i.e., with a large viewing angle). As a result of this path, microwaves in the attenuating layer (troposphere) of the atmosphere are attenuated less than for Earth-based radar. This circumstance modifies the optimum wavelength choice in the direction of much shorter waves (ref. 4A-1).

The classical radar equation and the radar equation for meteorological targets are necessary not only to determine the attainable values of the radar parameters but also to guarantee complete coverage of the Earth surface. To do so requires the utilization of a system of four radar-equipped satellites (ref. 4A-1).

A series of about 10 echo pulses must be received. The number of these pulses N_r is determined by the pulse repetition frequency f_p, the scanning speed of the beam V_γ, and the width of the antenna radiation pattern in the vertical plane θ_2.

$$N_r = 0.5\,\frac{f_p\theta_2}{V_\gamma} \qquad (4A\text{–}5)$$

The value of f_p is limited by the average transmitted power and the maximum operating range of the radar. Because of the first condition, the permissible value of f_p must be selected as $f_p \leq \bar{P}/(P_t t_p)$, where $\bar{P}$ is the average power and t_p is the radar pulse duration.

With present-day transmitters, $\bar{P} \approx 300$ W. Because the optimum wavelength for meteorological radars in satellites appears to be $\lambda = 2$ to 3 cm (ref. 4–9), $P_t \approx 3\times10^5$ W. The duration of the transmitted pulse T, to achieve the desired resolution, must be equal to 1 μsec. Then $f_p \leq 10^3$ Hz.

The second condition is concerned with the maximum radar range. In this case (with f_p in hertz)

$$\frac{1}{f_p} \gg \frac{2R_m}{c} \qquad (4A\text{–}6)$$

and

$$f_p \leq \frac{1.5\times10^5}{R_m} \qquad (4A\text{–}7)$$

For the satellite radar with pencil beams, meteorological targets will be detected within the range interval of 30 to 40 km, even with large scanning angles, because they are located in the troposphere. Consequently, to obtain readings of distance relative to the surface of the Earth, it may be assumed that $R_m = 30$ km. Then, $f_p \leq 5\times10^3$ Hz. However, the possibility of obtaining received echoes at the time the radar transmitter is turned on must be considered. It is easy to show that pulses, transmitted at a frequency of 600 Hz, will not be received from a range of 500 km each second pulse. With $f_p = 1200$ Hz, the echo will not be received on every fourth pulse, and so forth. To set the "blind" zone beyond the limit R_m, it is possible, for example, to take $f_p = 1000$ to 1150 Hz. Then, $\bar{P} = P_t f_p t_p = 3\times10^5\times1150\times10^{-6} = 345$ W.

Returning to equation (4A–5), in which

the scanning speed V_γ enters, one can show that

$$V_\gamma = \frac{2\gamma_s V_{pr}}{0.8\theta_1 H} \qquad (4A\text{–}8)$$

where γ_s is the scanning angle and θ_1 is the width of the radiation pattern in a plane perpendicular to the plane of the orbit. From equations (4A–5) and (4A–8)

$$\theta_1\theta_2 = \frac{4N_r\gamma V_{pr}}{0.8 f_p H} \qquad (4A\text{–}9)$$

The satellite velocity of motion projected on the Earth surface V_{pr} is related to its velocity of rotation around the Earth V_{kr} by

$$V_{pr} = \frac{V_{kr}R_E}{R_E+H} \qquad (4A\text{–}10)$$

with

$$V_{kr} = \frac{2\pi(R_E+H)}{T_s} \qquad (4A\text{–}11)$$

where T_s is orbital period in seconds.

Equation (4A–10) does not take into account the Earth rotation V_e. Generally, the receiving antenna beam along the Earth has a velocity

$$\mathbf{V} = \mathbf{V}_{pr} + \mathbf{V}_e \qquad (4A\text{–}12)$$

The magnitude of the vector velocity is

$$V = R_E\Omega_e \cos\phi \qquad (4A\text{–}13)$$

where Ω_e is the angular velocity of the Earth rotation, and ϕ is the terrestrial latitude of the subsatellite point.

For satellites with circular polar orbits

$$V_{pr} = [(V_{kr})^2 + (V_e)^2]^{\frac{1}{2}} \qquad (4A\text{–}14)$$

Analysis of equation (4A–9) shows that the necessary width of the radiation pattern also depends on the required angle of scan, the orbit height, and the number of pulses transmitted and received.

The scanning angle γ_s and the distance from the satellite to the Earth depend on the orbit height, the required longitudinal angular width of the coverage, and the number of satellites. The widths of the radiation pattern $\theta_1\theta_2$ are also determined by these parameters. This limits the use of narrow radiation patterns for the purpose of achieving large detection range and satisfactory resolution.

As an example, consider a single search of the Earth surface with four satellites with $N_r=10$ pulses, $\gamma=78°$, $H=400$ km, $f_p=1150$ Hz, and $V_{pr}=7.2$ km/sec. Substituting in equation (4A–9) yields $\theta_1\theta_2=1.78°$. This is achieved with $\theta_2=0.51°$ and $\theta_1=3.5°$.

With the indicated radar characteristics from the radar equation by Stepanenko (ref. 4–12), the ratio of the received power to the transmitter power for a detection probability of 0.9 can be readily obtained. Then

$$\frac{P_r}{P_t} = 5.2\times10^{-6}\frac{Z}{R^2}kk_z \qquad (4A\text{–}15)$$

where R is given in km, Z is in mm^6/m^3, and k is the attenuation factor.

According to experiments, the radar reflectivity Z is different for various atmospheric conditions and varies within the limits $10^{-3}\ mm^6/m^3 \leq Z \leq 10^6\ mm^6/m^3$.

Then, with $R=400$ km, the beam filling factor $k_z=0.3$, and the attenuation factor $k=0.5$, the ratio P_r/P_t will vary from 5×10^{-25} to 5×10^{-16}. For $R=1000$ km, $7.8\times10^{-26} < P_r/P_t < 7.8\times10^{-17}$.

If the radar receiver sensitivity is taken to be $P_{min}=10^{-14}$ W and the transmitter power $P_t=300$ kW, then $P_r/P_t=3.3\times10^{-20}$ (ref. 4A–2). Comparing this ratio with the required ratio of P_r/P_t for clouds and rain, one can determine those regions of rain that are detectable from satellites. Presently, clouds without rain cannot be detected with radar methods from satellites because the great distances result in a very small ratio of P_r/P_t. Increasing this ratio to insure the possibility of detecting nonrain clouds and measuring their upper height is possible with passive infrared radiometer methods.

Analysis of table 4A–I shows that, with a 400-km orbit, it is possible to detect moderate and heavy rain within the range of coverage.

UTILIZATION OF RADAR WITH FIXED, PLANAR RADIATION PATTERNS

This type of pulse radar is of interest because of the simpler antenna construction and the greater number of pulses on target.

TABLE 4A–I.—*Maximum Detection Ranges of Clouds With Pulse Radar of Selected Characteristics*

Characteristic	Maximum detection range, km			
	200	400	600	800
k_z	0.5	0.3	0.1	0.08
Z_{min}, mm^6/m^3	64	415	2880	5100
I_{min}, mm/hr [a]	.46	1.50	5.08	7.25

[a] I_{min}=minimum detectable intensity of rain.

Coverage of the Earth surface with such a satellite is obtained with two fixed, planar beams oriented perpendicular to the orbit plane of the satellite.

The radar has the following parameters: wavelength of 3 cm, radiated pulse power of 300 kW, receiver sensitivity of 10^{-14} W, pulse width equal to 4 to 5 μsec, angular width of the radiation pattern in the horizontal plane $\theta_1=0.23°$, and angular width of the radiation pattern in the vertical plane $\theta_2=30°$.

The radar has two antennas that are alternately switched to the receiver-transmitter. The frequency of switching is

$$F_{pod}=1.9\times10^{-6}\,\theta_1 h(H+R_E)\left(1+\frac{H}{R_E}\right)^{1/2}k_{per} \qquad (4A\text{–}16)$$

where k_{per} is the coefficient of overlap.

With $H=400$ km, the value of $F_{pod}\approx 16$ Hz. The width of the radiation pattern θ_1 is selected to obtain sufficient antenna gain, subject to the manufacturing restriction that $D_a/\lambda=300$, where D_a is antenna diameter. The width of the radiation pattern $\theta_2=30°$ insures complete coverage of the Earth surface with four satellites at an orbit height of 400 km.

One of the disadvantages of fixed planar beams is that unwanted clutter is almost always reflected from the sea or the Earth surface, together with the desired echoes from clouds and rain. These reflections create background that makes it difficult to extract the signals from the meteorological targets that are of interest.

In this case, the minimum detectable intensity of rain I_{min} (in mm/hr) can be expressed by the following relationship (ref. 4–12) :[1]

$$I_{min}=\left(\frac{8\pi\theta_1\theta_2^2\lambda^2R_m^3m_1P_r+m_2P_t\lambda^4h\tan\beta\,S(\beta)\,k}{\alpha 8\pi\times10^{-16}\,P_t h\theta_2R_m k k_z}\right)^{1/\gamma} \qquad (4A\text{–}17)$$

TABLE 4A–II.—*Calculation of* I_{min} in mm/hr *According to Equation (4A–17)*

Condition	Maximum detection range, km			
	300	400	500	600
Without clutter	1.5	2.0	2.8	3.4
Clutter from land	9.1	8.0	7.0	7.3
Clutter from water surface	2.0	3.1	2.8	3.7

Using the previously mentioned radar characteristics and with $m_1=m_2=1$, $k_z=5\times10^{-2}$, $k=0.4$, $\alpha=220$, and $\gamma=1.6$, one can determine with equation (4A–17) the value of the rain intensity with $\beta=40°$ and the scattering coefficient $S(\beta)=10^{-1.8}$, corresponding to a grass-covered ground; and $S(\beta)=10^{-3.4}$, corresponding to a water surface (table 4A–II).

Analysis of the table shows that the contribution of the clutter is substantial. However, the minimum detectable rain intensity is increased three to six times compared to the rain intensity in the absence of clutter. The characteristics are such that, in the presence of clutter, the minimum detectable rain becomes less, despite the increased range. This is explained by the fact that the echo signals from volumetric meteorological targets decrease as the square of the range, and the echoes from the area targets as the range cubed.

These calculations show that, with an increase in the angle of sighting β, the contribution of the clutter increases because of an increase of the multiplier $\tan\beta$ in the second term of the numerator of equation (4A–17).

In such a manner, the effectiveness of

[1] *Translator's note:* The quantity γ has a different meaning in eq. (4A–17) than it does in eq. (4A–9).

radar with planar beams for detecting meteorological targets from satellites is degraded by the harmful effect of the Earth surface.

To increase the effectiveness, it is necessary to attempt to reduce the effect of the ground reflection. To a large degree, this problem can be solved by using a multiwavelength radar.

In the microwave region, the scattering coefficient of the Earth surface $S(\beta)$ and, consequently, the effective scattering area are weakly dependent on the wavelength; but for rain, the scattering coefficient is proportional to λ^{-4}. This effect can be used to remove the significance of ground clutter.

The difference of the minimum received signals is

$$P_{\lambda_1 \min} - P_{\lambda_2 \min} = m_1 P_{\lambda_1 sh_1} + m'_1 P_{\lambda_1 e} - m_2 P_{\lambda_2 sh_2} - m'_2 P_{\lambda_2 e} \quad (4A\text{–}18)$$

Let the noise powers $P_{\lambda_1 sh_1}$ and $P_{\lambda_2 sh_2}$ and also the coefficients of the distinction be the same. Then, according to the theory of radar reception, the difference of the internal noise increases by $\sqrt{2}$.

To effectively use this method, it is necessary for the radiation patterns at both wavelengths to be the same. Accordingly, they will have the same angular resolution and filling factor k_z.

Substituting in equation (4A–18) the relationship in equation (4A–17) and calculating its relative rain intensity, the following expression is obtained:

$$I_{\min} = \left(\frac{1}{\alpha 64\pi^2 \times 10^{-19} \, h k_z \left(\frac{P_{t_1} k_1}{\lambda_1^2} - \frac{P_{t_2} k_2}{\lambda_2^2} \right)} \left\{ \sqrt{2}\, P_{\min} R_m^2 \theta_1 \theta_2 + \frac{h \tan \beta [S_1(\beta) \lambda_1^2 P_{t_1} k_1 - S_2(\beta) \lambda_2^2 P_{t_2} k_2]}{8\pi \theta_2 R_m} \right\} \right)^{1/\gamma} \quad (4A\text{–}19)$$

An analysis of this formula reveals that, with other conditions equal, the sensitivity of the dual-wavelength radar will increase with the difference in the denominator of the multiplying term and will decrease with the difference in the numerator of the second sum of the braces.

As one version of a dual-wavelength radar, an instrument was examined that operated at wavelengths of $\lambda = 0.8$ cm and $\lambda = 3$ cm. The main reason for selecting these bands was that, at these wavelengths, detailed scattering coefficient data $S(\beta)$ are available for various surfaces of the Earth with various viewing angles.

Solving the equation for $I_{\min}$ with $P_{t_1} = 300$ kW, $P_{t_2} = 30$ kW, $k_1 = 0.2$, and $k_2 = 0.4$ and assuming the other radar parameters are the same as before, the values in table 4A–III are obtained for the minimum detectable intensity of rain.

A comparison of the values of tables 4A–II and 4A–III reveals the advantage of two-band radar.

In addition to the detection of rain, an interesting problem is the possibility of measuring its intensity from satellites. Although the solution of this problem depends on overcoming a series of difficulties connected with the necessity to automatically process and measure the backscatter signal power under space conditions, the achievements of electronics and processing systems design offer hope for successful use of spaceborne two-band meteorological radar in the coming years for the detection of storms and for the measurement of rain. In this regard, it is tempting to present the possibility of installing such meteorological radars on geostationary satellites at orbit heights of 35 700 km.

Using equation (4A–15) (the radar equation) with a beamwidth $\theta = \lambda/D_a = \lambda/400 \approx 0.0025$ rad, $P_t = 3 \times 10^5$ W, $I_{\min} = 4$ mm/hr, $P_{\min} = 10^{-15}$ W, $t_p = 1$ μsec, attenuation coefficient $k = 0.5$ at $\lambda = 2$ cm, $k = 10^{-1}$ at $\lambda = 0.8$ cm, $k = 10^{-3}$ at $\lambda = 0.3$ cm, and with the value $k_z = 0.3$, the following required values for P_r/P_t are obtained.

For λ equal to 0.3, 0.8, and 2 cm, the cor-

TABLE 4A–III.—*Minimum Detectable Intensity of Rain (mm/hr) With Two-Band Radar*

Surface	Maximum detection range, km	Depression angle to near edge of coverage, deg			
		10	30	50	70
Land	300	0.5	1.8	3.6	4.0
Sea		.42	.42	.42	.42
Land	400	0.76	1.76	3.16	3.5
Sea		.7	.7	.7	.7
Land	500	0.95	1.73	2.9	3.1
Sea		.93	.93	.93	.93
Land	600	1.2	1.79	2.8	3.0
Sea		1.16	1.16	1.16	1.16

responding ratios of P_r/P_t are 5×10^{-21}, 7×10^{-20}, and 5.9×10^{-20}. At this time, the technically achievable values of these ratios appear to be $P_r/P_t=10^{-15}/(3\times10^5)\approx 3.3\times10^{-21}$. Thus, it appears that areas of rain will be detected from satellites at λ equal to 0.8 and 2 cm. With the selected values of θ and t_p, the geometrical resolution in the tangential dimension amounts to 80 to 90 km; and, in the radial direction, the measurements are from 6.5 to 0.2 km, with angle of scan γ_s increasing from 0.2° to 7°.

REFERENCES

4A–1. KMITO, A. A., ET AL.: Systems for Receiving and Transmitting Meteorological Information. Gidrometeoizdat (Leningrad), 1971.

4A–2. DOMBKOVSKAYA, E. P.: Determination of Sea Surface Temperature and Atmospheric Humidity From Satellite Measurements of the Thermal Radio Emission of the Earth-Atmosphere System. Satellite Meteorology, V. G. Boldyrev and N. F. Veltishchev, eds., Gidrometeoizdat (Leningrad), 1969.

C. 5